THE EFFECTS OF RIDGE WIDTH ON InGaAsP QUANTUM WELL LASERS

THE EFFECT OF VARYING THE RIDGE WIDTH

ON THE PROPERTIES OF

STRAINED LAYER InGaAsP-InP QUANTUM WELL LASERS

By

GREGORY LETAL

A Thesis

Submitted to the School of Graduate Studies

in Partial Fulfilment of the Requirements

for the Degree

Master of Engineering

McMaster University

MASTER OF ENGINEERING (1996)
(Engineering Physics)

McMaster University
Hamilton, Ontario

TITLE: The Effect of Varying the Ridge Width on the Properties of *InGaAsP* Strained Layer Quantum Well Lasers.

AUTHOR: Gregory Letal, B.Sc. (University of Alberta)

SUPERVISOR: Professor J.G. Simmons

NUMBER OF PAGES: xiii, 76

ABSTRACT

A study has been conducted to examine the effects of varying the ridge width on the operating characteristics of a strained-layer ridge waveguide *InGaAsP-InP* multiple-quantum well laser structure. A simple analytical model has been developed to explain how the input current required to reach a selected operating point changes with ridge width. It has been shown that a large portion of the current injected into the laser (as much as 60% for a 1.5µm ridge) escapes laterally from the active region. This model has been applied to lasers made from a wafer grown with 9 strained *InGaAsP* quantum wells on an *InP* substrate. The lasers themselves have a cavity length of 250µm and seven ridge widths ranging from 1.5µm to 5µm. The base temperature range investigated was from -40°C to 80°C. It has been shown that the diffusion length of the carriers within the laser decreases both with increased temperature and increased pumping. As well, the average current density in the active region at a specific operating point increases super-exponentially with temperature. The above-threshold characteristics were also examined from which the effects of the lateral current flow on the external differential efficiency were extracted. Lateral current changes little with external pumping so its effect on the differential external efficiency is minimal.

ACKNOWLEDGEMENTS

Dr. Simmons, my supervisor, is the first person I would like to thank. His courses and research suggestions have all been extremely helpful in the completion of this Master's thesis. He is a fountain of information, and fortunately, some of it has flowed in my direction.

There is no way I could forget John (a.k.a. Jack) Evans. Thank you for keeping me on my toes, providing me with useful suggestions, and acting as a liaison with Bell Northern Research. I would also like to thank him and Tony Vetter for constructing the experimental apparatus used to measure the laser characteristics. As well, I would like to thank Kelvin Prosyk and John Hazell for demonstrating how to use the equipment.

Dr. Jessop helped to decrease the complexity of this project by providing a computer program which calculated the optical modes within a multiple-layer slab-waveguide, so he also deserves thanks.

I would also like to thank the people at Bell Northern Research. Without them, this study would not have been possible.

It appears that saying thanks to your family is a requirement within the acknowledgements. However, that is not the only reason why I am mentioning them here. They have always been supportive of my decisions and willing to help me out whenever I might need it so they deserve special thanks.

Finally, I would like to thank all the residents and visitors of my office for all the stimulating conversations (not all of which had to do with research). Combined, they make up a great information base as well as an interesting group of friends.

TABLE OF CONTENTS

Glossary

A_j	Forward propagating wave in the slab waveguide.
B_j	Backward propagating wave in the slab waveguide.
d	Active region thickness.
D_a	Ambipolar diffusion coefficient.
D_{eff}	Effective diffusion coefficient.
D_n	Diffusion coefficient for electrons.
D_p	Diffusion coefficient for holes.
E	Electric field due to the optical mode.
E_g	Band-gap energy of the semiconductor.
G	Carrier generation rate.
h	Planck's constant.
H	Magnetic field due to the optical mode.
I_{in}	Injected current into the active region.
I_L	Lateral current.
I_{th}	Current required to reach the threshold of the laser.
j	Layer number in the slab waveguide.
J'	Average current density beneath the ridge.
J_n	Current flowing laterally due to holes.
J_{nin}	Electron current into the active region.
J_p	Current flowing laterally due to electrons.
J_{pin}	Hole Current into the active region.
J_{in}	Injected current density through the top of the ridge ($I_{in}/(L_c \cdot W)$).
k_{jx}	Propagation constant in the x direction for the j_{th} layer.
L_c	Length of laser cavity.
L_D	Diffusion length.
L_{D1}	Diffusion length beneath the ridge.
L_{D2}	Diffusion length outside the ridge.
n	Electron carrier density.
n	Number of the top layer of the slab waveguide.
n_{je}	Index of the layer in the x direction.
n_{jo}	Index of the layer in the y and z direction.
p	Hole carrier density.
P	Power out of one facet of the laser.
q	Electronic charge.
R	Rate of photon escape out of one facet.
R_j	Position of the layer boundary (x=R_j).
R_m	Facet reflectivity.
W	Width of the ridge.
x	Lateral direction of the semiconductor laser.
z	Transverse (growth) direction of the laser.
α_{int}	Internal optical losses.

Γ	Optical confinement factor.
η_d	Single Facet external differential efficiency.
η'_d	Single Facet external differential efficiency with I_L removed.
η_i	Internal differential efficiency.
ε_o	Free-space permittivity.
λ	Wavelength of light in the semiconductor.
μ	Relative permeability (μ=1 in air).
μ_p	Mobility of holes.
μ_n	Mobility of electrons.
μ_o	Free-space permeability.
ν	Frequency of the light.
ξ	Electric field in the semiconductor.
τ	Carrier lifetime.

LIST OF FIGURES

LIST OF TABLES

CHAPTER 1: INTRODUCTION

1.1 BACKGROUND

The information age is upon us! Or at least, that is what we are being told by the media. The modern consumer desires access to information whether it is by exploring the World Wide Web or accessing pay-per-view television. Due to the large bandwidth required, optical fibres are one way that this growing desire for access to information could be satisfied. However, cost is a prohibitive factor to implementing a fibre-to-the-home communication system. A large portion of this cost is found in the packaging of the devices. If one was to develop a laser with an extremely low temperature sensitivity and which generates little heat during operation, the relatively expensive thermoelectric coolers that are currently part of the package could be omitted. Because of this, there is a large push to understand and remove loss mechanisms and other undesirable characteristics which result in heat generation. A loss in a semiconductor laser is defined as any mechanism which causes a carrier to recombine in a way which does not contribute to gain of the optical mode. It is the removal of loss mechanisms that has been driving the design changes of semiconductor lasers.

1.2 LOSS MECHANISMS IN SEMICONDUCTOR LASERS

Several carrier-loss mechanisms depend on both the type and the quality of material, but others can be greatly reduced by choosing an appropriate structure. Losses can be divided into two broad categories: optical losses and carrier losses, with the focus of this thesis being on carrier losses. Discussions about carriers in semiconductor materials require the consideration of both negative particles and positive vacancies (electrons and holes). For the electrons and holes to propagate in a crystal, they can only have certain values of energy and momentum which can be described by energy bands. The electrons reside in the conduction band and the holes reside in the valence band. In the III-V compounds, which are semiconductors that are commonly used today for lasers, there is one conduction band and three valence bands: the heavy hole, the light hole, and the split-off band as shown in Fig. 1.1. To produce light from a semiconductor, it is necessary for a hole in the valence band to occupy the same position as an electron in the conduction band. At such a time, there is a finite probability that the hole and electron will recombine. Since the two bands can be of different energy and momentum, either photons, phonons, or a combination of the two must be produced when the carriers recombine. This is required to satisfy both energy and momentum conservation. In an ideal case for a semiconductor laser, the electrons and holes will recombine to emit photons. If one was to add mirrors (which can be as simple as cleaved facets), a cavity in which stimulated emission can occur is created and a semiconductor laser is formed.

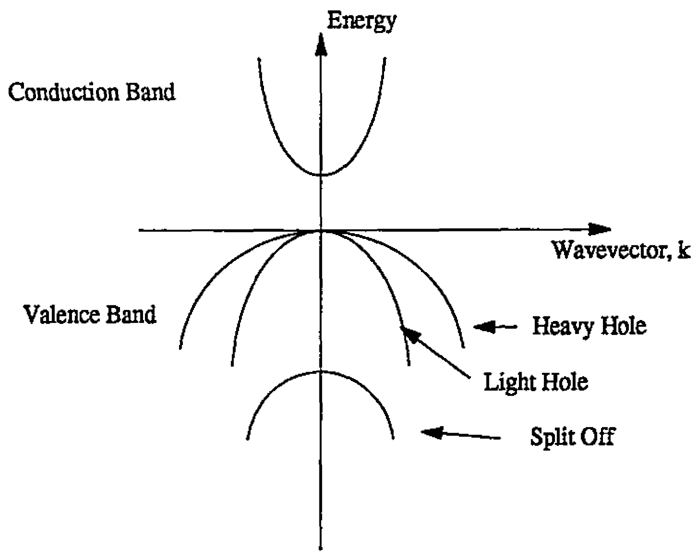

Fig. 1.1 Typical Band Diagram of a semiconductor used in a laser. (Assuming parabolic bands.)

There are several possible reasons why the electrons and holes might not recombine radiatively to produce stimulated emission in a semiconductor laser. One possibility is a material dependent loss. The main material dependent losses are: Shockley-Read (non-radiative) recombination and Auger recombination [Agrawal, 1993, p.98]. Shockley-Read recombination occurs when a material defect (trap) exists at an energy level within the band gap. As shown in Fig. 1.2, it is possible for a carrier to make transitions of less than the band gap and emit phonons instead of making one large transition and emitting a single photon. Auger recombination is a completely different process. It occurs when the electrons in the conduction band and the holes in the valence band recombine but instead of emitting a photon, they recombine in a way such that the energy is absorbed by another electron to push it into a higher band [Agrawal, 1993, p.98]. Both mechanisms result in carriers losing energy without producing photons, which is detrimental to laser performance.

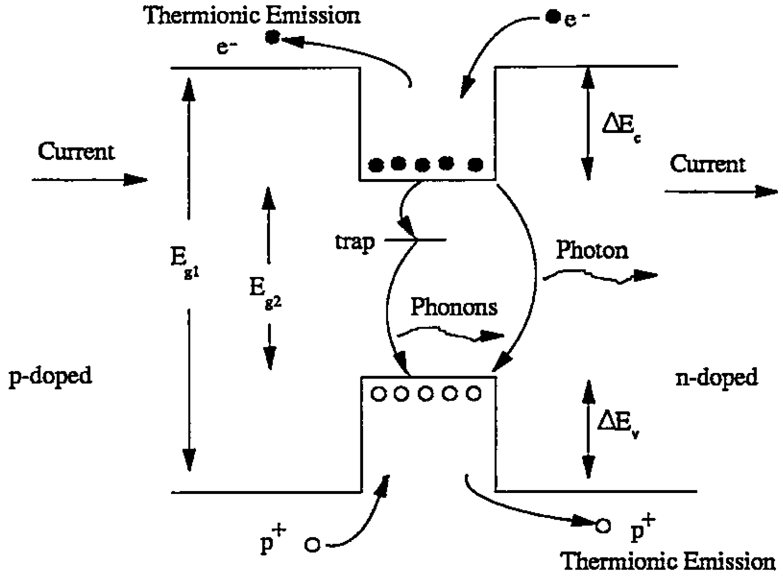

Fig. 1.2 Recombination processes and losses in double heterostructures.

The other type of loss in semiconductor lasers is structure dependent. Since recombination requires holes and electrons to occupy the same physical space, it is apparent that the amount of recombination would increase with an increase in carrier density. An elegant method of increasing the carrier density is by using a double heterostructure. This is where a slab in the middle of the semiconductor is replaced with another material of a smaller band gap. This causes an energy well to be formed in which electrons and holes can become trapped as shown in Fig. 1.2. The resulting increase in the carrier density improves the probability of recombination of holes and electrons so smaller currents are required for lasing. Carriers will still escape from this well by processes such as thermionic emission or Auger recombination, but the number of carriers escaping is greatly decreased and hence, the efficiency of the device is increased [Agrawal, 1993, p.3].

The concept of a double heterostructure was improved further by the introduction of the quantum well laser. If the material within the double heterostructure layer is thin enough, it is possible for quantum effects to dominate and the carriers will become trapped in discrete levels as illustrated in Fig. 1.3. This is the principle of a quantum well. The quantum well allows for a lower threshold current, and the improvement of many other laser performance characteristics.

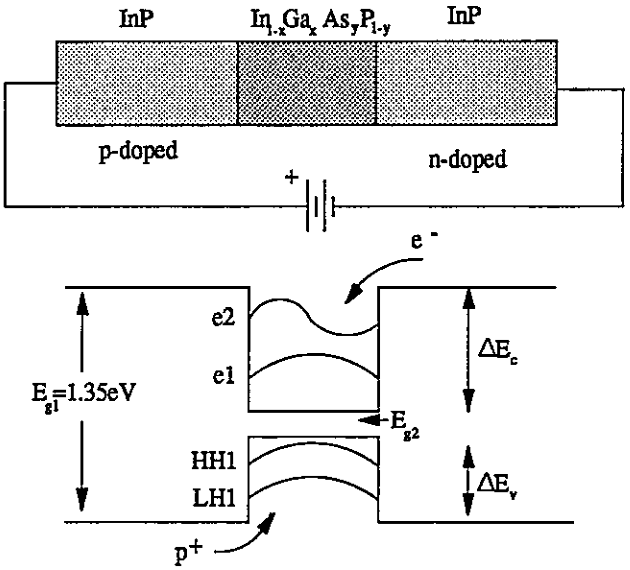

Fig. 1.3 Illustration of how different band gap semiconductors could be used to produce a quantum well.

It was soon discovered that the characteristics could be improved even further by adding strain to the quantum well material [Zory, 1993]. Strain can be used to modify the relative energy positions and shapes of the energy bands within the semiconductor as illustrated in Fig. 1.4. This can have the effect of: changing the wavelength emitted,

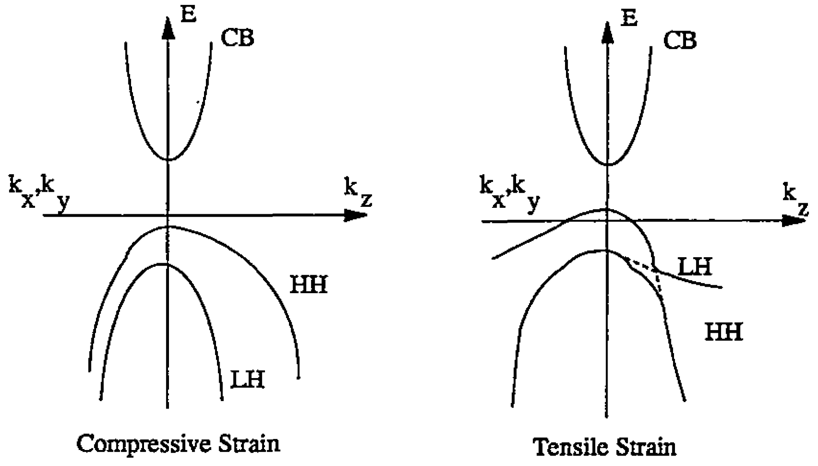

Fig. 1.4 Illustration of the effect of strain on the energy bands of a semiconductor.

changing the polarization of the emitted light, improving efficiency by modifying the effective mass of the holes, and reducing loss mechanisms such as Auger recombination [Zory, 1993, pp. 329-335]. Strain is formed by growing the quantum well material within a barrier material which has a different lattice constant. After growth, if the quantum well layers are thin enough, the material will distort to match the lattice constant found in the plane of the well (which is commonly the lattice constant of both the substrate and the barriers). If the quantum well material is grown larger than a certain critical thickness, strain relief through the formation of defects will occur in the material [Zory, 1993, p.372]. This places a limitation on both the amount of strain and the size of the well. Strained-layer semiconductor lasers are currently used by the communications industry, however much characterization and optimization is still required.

The double heterostructure and quantum wells perform well at confining the carriers in the transverse direction but do not impede the lateral current flow. This provides a potential problem for some laser designs. The most common type of laser used for communication purposes is the ridge waveguide laser because it is relatively easy to manufacture while, at the same time, being relatively efficient. The main alternatives are the stripe contact laser or the buried heterostructure laser. Illustrations of the various structures are shown in Fig. 1.5. The ridge provides lateral confinement of the optical mode which makes it more efficient than a stripe contact laser. As well, it is constructed simply by etching a ridge in the top layer of the laser which is a much easier and more reliable process than the etching and regrowth required to construct a buried heterostructure laser. This simplicity has a cost however. The ridge waveguide laser does not contain any lateral carrier confinement structure other than the fact that the ridge is of a limited width. This lateral current spreading, as illustrated in Fig. 1.6, could easily be a large loss mechanism since there is no barrier to impede the current flow. This thesis is an attempt to measure the magnitude of this loss mechanism.

1.3 LASER CHARACTERISTICS

1.3.1 Threshold Current

There are several characteristics that are common to most semiconductor laser L-I (Light-Current) graphs, a sample of which is illustrated in Fig. 1.7. By examining the curve, it can be seen that there are two nearly linear regions, one of a low slope, and

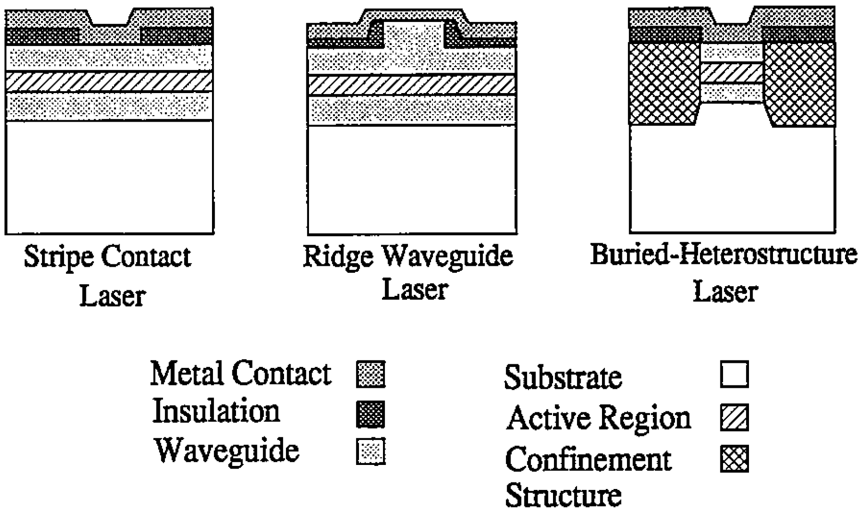

Fig. 1.5 Illustration of various laser structures.

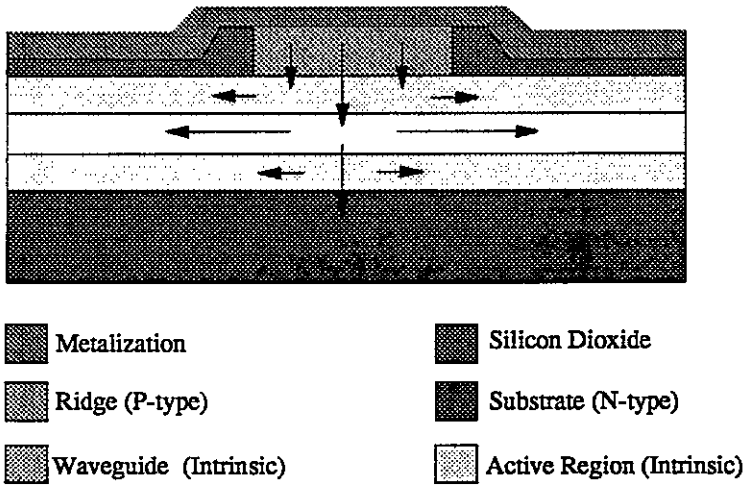

Fig. 1.6 Illustration of lateral current spreading in a ridge waveguide laser.

another of a steep slope separated by a region of high curvature. The knee in the curve is called the threshold of the laser and is the point where the dominant emission process switches from spontaneous to stimulated. For most laser applications, one wishes to have as low of a threshold as possible since the current injected to achieve threshold does not contribute usefully to the output. There are two techniques that are commonly used for determining threshold. One is by extrapolating the linear portion of the above threshold portion of the graph down to the axis and calling the intercept threshold as illustrated in Fig. 1.7 as I_{thl}. In this situation, one can write:

$$R=\frac{\eta_d}{q}(I_{in}-I_{th}) \tag{1.1}$$

which relates the number of photons escaping out of one facet each second, R, to the input current, I. The term η_d is defined as the single facet differential (external) efficiency and is given by

$$\eta_d=\frac{q}{hv}\frac{dP}{dI_{in}} \tag{1.2}$$

and will be discussed in greater detail shortly. In (1.2), h is Planck's constant, q is the electronic charge, ν is the frequency of the light emitted by the laser, and $P(=R\cdot h\cdot\nu)$ is the power emitted from a single facet. The slope of the curve (dP/dI_{in}) is evaluated on the linear portion of the L-I curve as illustrated in Fig. 1.7.

In situations of low external efficiency or a large amount of spontaneous emission, I_{thl} can deviate a large distance from the knee of the graph. An alternate method of calculating the threshold is by extrapolating the linear spontaneous and stimulated emission regions of the L-I curve to find the intersection which is illustrated in Fig. 1.7

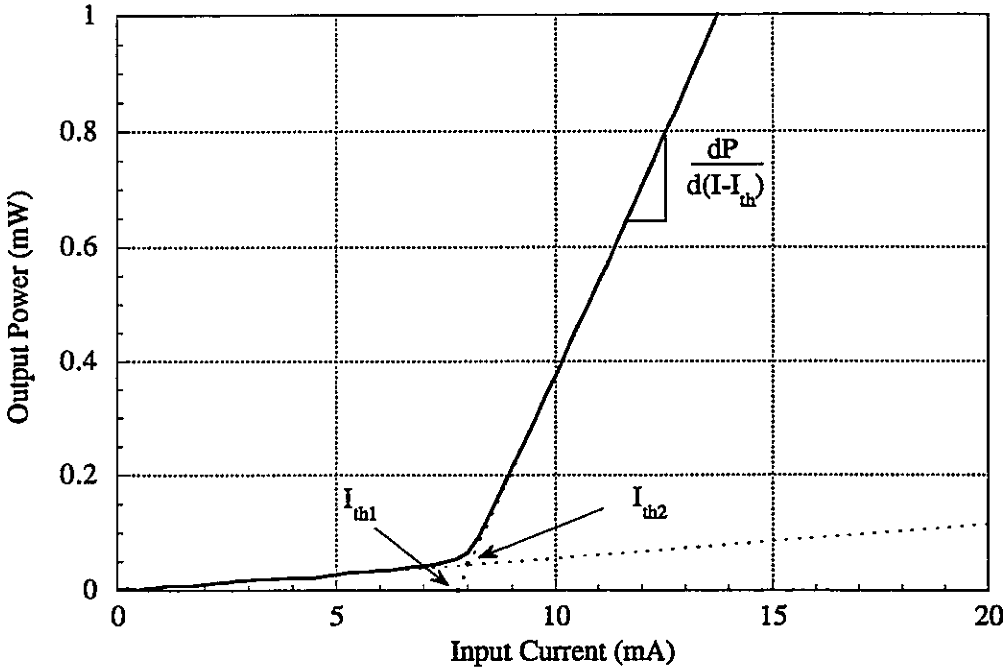

Fig. 1.7 A sample L-I Curve shown for a 1.5μm laser at -40°C.

as I_{th2}. This method ensures that the threshold point chosen is close to the knee of the curve and, hence, was the method of choice for this thesis. Even so, these two methods are approximately equivalent provided the amount of spontaneous emission is small.

1.3.2 Differential Efficiency

The above-threshold, linear portion of the L-I curve is also of interest, since from it, one can calculate the differential efficiency (η_d) as previously given by (1.2). The differential efficiency is simply the change in the number of photons over the change in the number of injected carriers. In general, one wishes to have as high of an external efficiency as possible.

Alternatively, one can examine the total external efficiency; this is simply the number of photons out divided by the number of carriers injected. Discussions about the total efficiency are not common since it would be necessary to quote a different value for each input current level of interest. The constant value obtained from the differential efficiency is not as awkward to deal with and provides a better insight into what is happening within the laser.

By using different lengths of lasers, it is also possible to calculate a characteristic property known as the internal quantum efficiency (η_i). It is a measure of the efficiency of converting carriers into photons. The common expression relating the internal and external efficiency is:

$$\eta_d = \frac{\eta_i}{2} \cdot \left[1 + \frac{\alpha_{int} L_c}{\ln(1/R_m)}\right]^{-1} \tag{1.3}$$

where α_{int} is defined as the internal optical loss, L_c is the length of the cavity, and R_m is the facet reflectivity [Agrawal, 1993, p.60]. The factor of two is required since the total number of photons emitted from the device must be considered in the calculation of the internal efficiency. However, in this thesis, η_d is defined as the single-facet differential efficiency since the output from only one facet is measured. By assuming that the two facets are identical, a factor of two appears in (1.3). In other works, η_d is sometimes used to represent the two-facet differential efficiency.

The internal quantum efficiency, as defined here, is also a differential type of efficiency and does not account for below-threshold losses. This means that normally η_i

has a value which is close to unity. This can be understood by realizing that most non-radiative loss mechanisms (such as Auger recombination and thermionic emission) depend on the carrier density. Since the carrier density is approximately constant above threshold, the magnitude of these losses will not change once threshold is reached. This suggests that it is possible to have a laser structure that has a large threshold current as well as an internal differential efficiency which is close to unity.

1.4 THESIS OBJECTIVE AND OUTLINE

Studies performed in the past have examined the various loss mechanisms in *InGaAsP/InP* quantum well, ridge waveguide semiconductor lasers. However, few (for example, Hu et al. [1994]) have examined the effects of lateral current flow on the threshold current, and even fewer have examined its effects on the above-threshold operation of the laser.

Chapter 2 discusses the optical confinement requirements in semiconductor lasers and the profile of the optical mode. Also discussed are techniques of calculating the optical mode profile for different types of waveguides.

Chapter 3 outlines the current continuity equations and simplifying approximations (such as ambipolar diffusion) which are commonly used to obtain solutions to these equations. A model is developed from these equations which allows the carrier profile in the lateral direction of a ridge waveguide laser to be calculated. From this carrier profile, an expression is derived for the lateral current. Next, the input current to the laser is expressed in terms of the average current density beneath the ridge, the width of the ridge, and the diffusion length of the carriers in the material. This expression is linked to the lateral current flow.

Chapter 4 describes the experimental apparatus and the results obtained from the application of the model to the data obtained from operating lasers of different ridge widths at various operating points. Also, the validity of the approximations made in the derivation of the model are examined. As well, the effects of the lateral current on laser operation at threshold and in the above-threshold regime are examined.

Chapter 5 describes the effect of lateral current on the external differential efficiency. The internal efficiency could not be calculated since different lengths of lasers were not available. The final calculations in this thesis describe an additional loss mechanism which is independent of pumping in the above-threshold regime and is speculated to be due to carriers recombining outside the active region. This is a transverse loss as compared to current spreading which is a lateral loss mechanism.

CHAPTER 2: OPTICAL CHARACTERISTICS OF WAVEGUIDES

2.1 INTRODUCTION

Semiconductor lasers require the optical mode to be confined to the active region of the laser. The active region must be designed so that confinement of the optical mode occurs in the both the lateral and transverse directions as illustrated in Fig. 2.1. In the transverse direction, the guiding occurs naturally because the active region has a higher index of refraction than the cladding regions. This allows for an optical waveguide to be formed with the same heterostructure used for carrier confinement. The optical guiding effect in the lateral direction, however, depends on the structure applied. This guiding structure can vary from a buried heterostructure made of materials of two different indices to a step etched in the cladding which forms a ridge waveguide.

2.2 MULTIPLE LAYER SLAB WAVEGUIDES

Laser structures consist of dielectric stacks which in addition to producing gain, act as a waveguide. There are several numerical techniques which can be used to find the optical mode profile in a multiple-layer slab waveguide. One such technique is known as the transfer matrix approach for slab waveguides and is the approach adopted in this thesis.

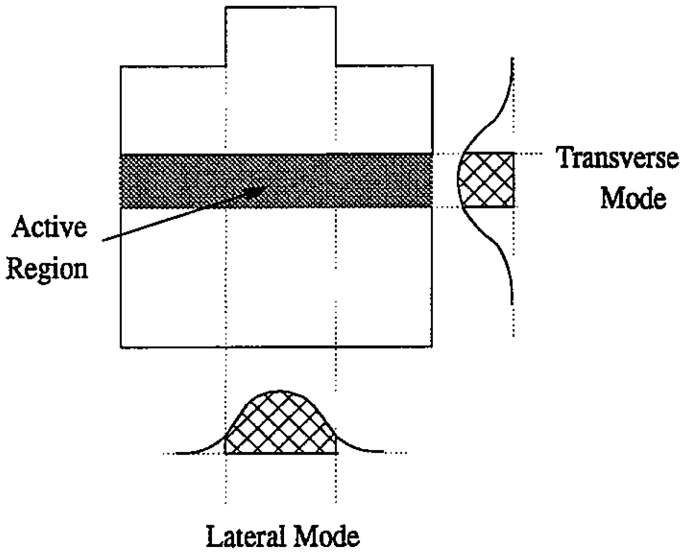

Fig. 2.1 Illustration of the lateral and transverse modes within a ridge waveguide.

The transfer matrix approach has been described in detail by Walpita [1985], so only a brief summary is given here. It can shown that for a slab waveguide one can write the matrices:

$$\begin{bmatrix} E_{jy} \\ i\omega\mu\mu_o H_{jz} \end{bmatrix} = \begin{bmatrix} \exp[-k_{jx}(x-R_j)] & \exp[k_{jx}(x-R_j)] \\ -k_{jx}\exp[-k_{jx}(x-R_j)] & \exp[k_{jx}(x-R_j)] \end{bmatrix} \cdot \begin{bmatrix} A_j \\ B_j \end{bmatrix} \tag{2.1}$$

for TE modes and

$$\begin{bmatrix} H_{jy} \\ i\omega\varepsilon_o E_{jz} \end{bmatrix} = \begin{bmatrix} \exp[-k_{jx}(x-R_j)] & \exp[k_{jx}(x-R_j)] \\ -\frac{k_{jx}}{n_{jo}^2}\exp[-k_{jx}(x-R_j)] & \frac{k_{jx}}{n_{jo}^2}\exp[k_{jx}(x-R_j)] \end{bmatrix} \cdot \begin{bmatrix} A_j \\ B_j \end{bmatrix} \tag{2.2}$$

for TM modes, where

j	represents the layer number
ε_o	is the free space permittivity
μ_o	is the free-space permeability
A_j	is the forward propagating wave
B_j	is the backward propagating wave
k_{jx}	is the propagation constant in the x direction
n	is the number of the last layer
R_j	is the position of the layer boundary ($x=R_j$)
n_{je}	is the index of the layer in the x direction
n_{jo}	is the index of the layer in the y and z direction and
μ	is the relative permeability (μ=1 in air).

The propagation constant of each layer k_{jx} can be re-expressed in terms of the propagation constant in the z direction, β, by the equations

$$k_{xj}=(\beta^2-k^2n_{jo}^2)^{\frac{1}{2}} \tag{2.3}$$

for a TE mode and

$$k_{jx}=\left(\frac{n_{jo}}{n_{je}}\right)^2(\beta^2-k^2n_{je}^2)^{\frac{1}{2}} \tag{2.4}$$

for a TM mode. The directions and numbering systems are illustrated in Fig. 2.2. By requiring the electric and magnetic fields to be continuous across the boundaries, one can write

$$\begin{bmatrix}A_n\\B_n\end{bmatrix}=\begin{bmatrix}\alpha_1 & \alpha_2\\ \alpha_3 & \alpha_4\end{bmatrix}\cdot\begin{bmatrix}A_1\\B_1\end{bmatrix} \tag{2.5}$$

where the α_k terms are the resultant values from the matrix multiplication. For the wave to propagate within the waveguide, the waves in the outer layers are required to be evanescent. This means that B_n and A_1, the coefficients of the backward and forward propagating waves at the boundaries of the outer dielectrics, must equal zero. For such a situation to occur, one must have α_4=0. By setting this matrix element to zero, numerical techniques can be used to solve the resulting function for the propagation constant, β, and, hence, the electric field profile within a dielectric stack. These techniques are used in the next section to determine the optical properties of the ridge waveguides used within the lasers of this thesis.

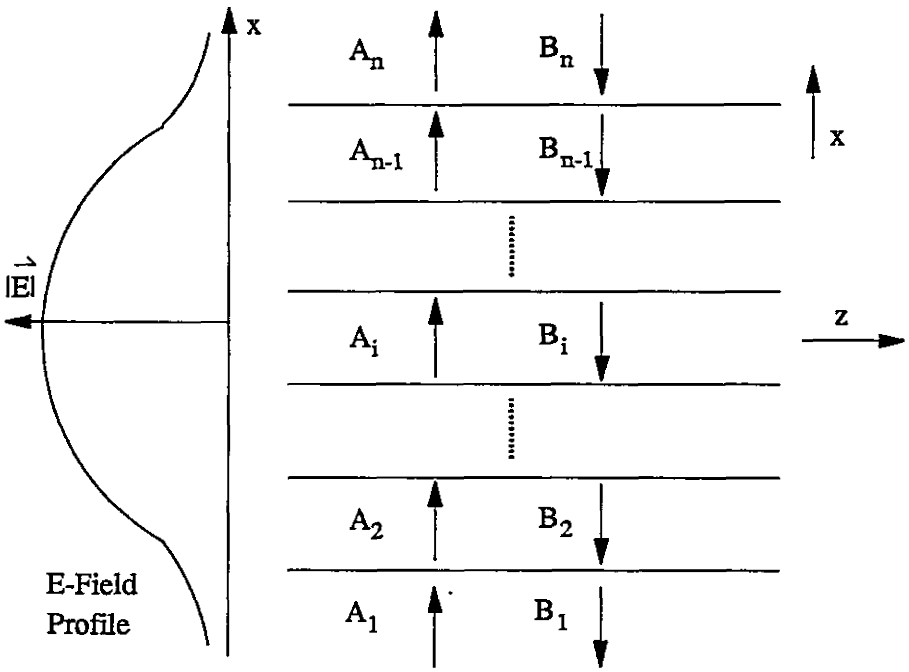

Fig. 2.2 Illustration of a multiple-layer slab waveguide depicting the numbering system used in the equations.

2.3 TWO-DIMENSIONAL WAVEGUIDE STRUCTURES

The laser structures that have been discussed (Fig. 1.5) all contain two-dimensional waveguides. In the ridge waveguide structure, the lateral guiding occurs due to an effective index change caused by the ridge [Tamir, 1975, p.64]. Solving for a multiple-layer slab-waveguide is not sufficient to find the complete mode profile within such a two-dimensional structure. To calculate the approximate optical mode profile of a waveguide, it is often possible to separate the profile into lateral and transverse directions.

The effective index method is a mathematical technique which separates the optical profile into lateral and transverse directions. This is done even though the problem is not truly separable. This approximation is valid whenever the thickness of the transverse guiding region (i.e., the active region) is much smaller than the width of the ridge. If this is the case, the calculation of the mode profile in the transverse direction is accomplished by using the multiple-slab waveguide calculation demonstrated in the previous section. (In this thesis, the transverse direction is defined as the direction of wafer growth.) The regions beneath and outside the ridge are treated as separate one-dimensional dielectric stacks. From the propagation constants, one can calculate an effective index of each of the dielectric stacks. More specifically, if β_i is the propagation constant of region *i*, then the effective index of a dielectric stack is given by:

$$n_{eff_i} = \frac{\beta_i \cdot \lambda}{2\pi} \tag{2.6}$$

This gives the effective index of each of the three regions illustrated in Fig. 2.3. These effective indices are then used to construct a three-layer slab waveguide for which it is a simple matter to calculate the optical mode. It is important to note that with this method, the calculated mode profile is only an approximation and differs from the actual solution away from the axis.

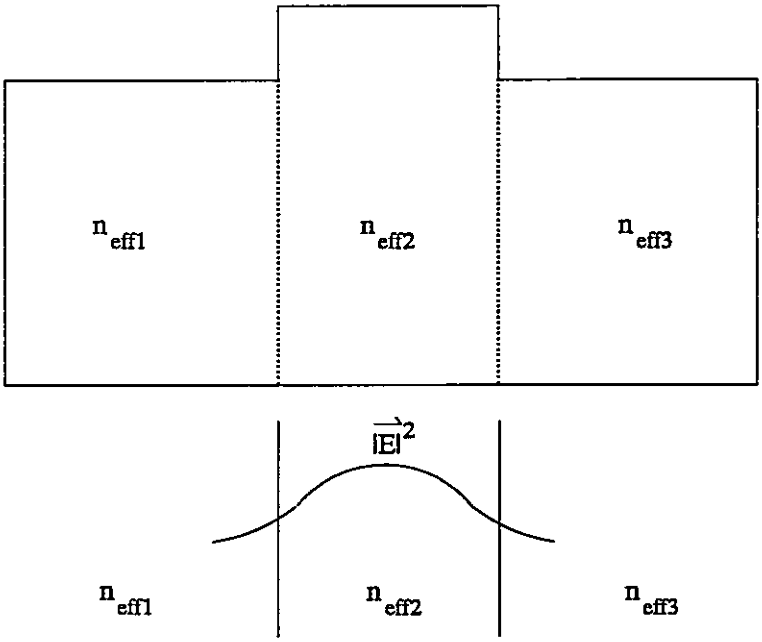

Fig. 2.3 Illustration of the effective index method.

2.4 OPTICAL CONFINEMENT

2.4.1 Optical confinement relating to a laser

Optical confinement is a term used to describe the fraction of the optical power which is confined to the active region of a laser. In the case of a quantum well laser, the optical confinement refers to the fraction of the optical power within the quantum wells in the transverse and lateral directions. The general equation used to calculate the confinement is:

$$\Gamma = \frac{\int_R E(x,y)^2 dA}{\int_{-\infty}^{\infty} E(x,y)^2 dA} \tag{2.7}$$

where E is the electric field. The top integral is taken over area R, the active region area. This equation is valid for any two-dimensional structure. In situations where the effective index method is valid, the optical confinement is often also separable into the two directions. In such a case, $\Gamma=\Gamma_x \cdot \Gamma_y$, where Γ_x and Γ_y are the confinement factors in the lateral and transverse direction respectively. When comparing the confinement factors of different ridge waveguide structures, it is therefore valid to only consider the lateral confinement since the transverse confinement is constant with respect to ridge width.

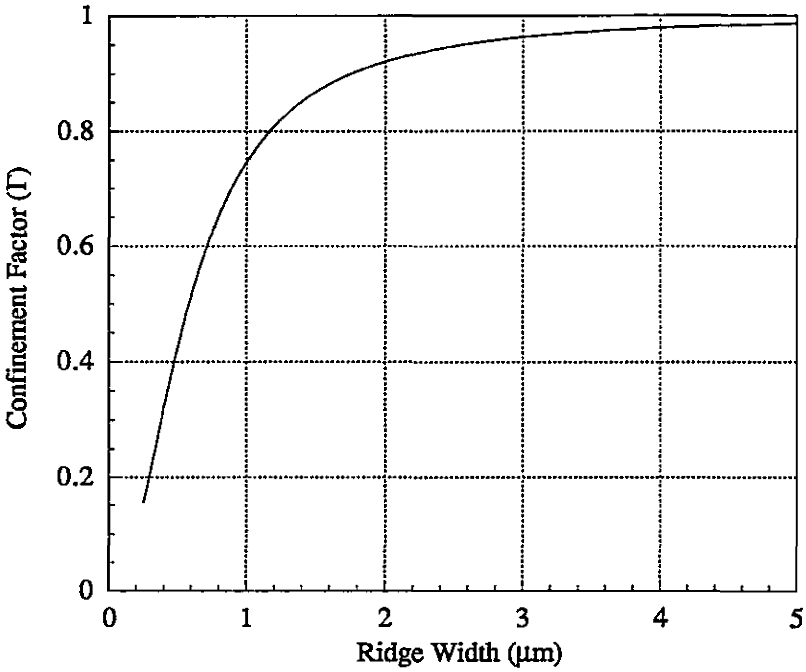

Fig. 2.4 The variation of the lateral optical confinement in a 3 layer slab waveguide with a centre layer index of 3.24 and a cladding index of 3.21.

2.4.2 Study of the Lateral Optical Mode Confinement

One of the main approximations made for the model presented in the next chapter is that the lateral optical mode is well-confined to the region beneath the ridge. To check this approximation, a cold cavity calculation of the lateral optical confinement was performed. In a cold cavity calculation, the effects of gain and the carrier concentrations on the refractive index of the materials are ignored. There is an analytical expression that can be used to calculate the approximate optical confinement of a three layer slab wave guide as described by Kapon [1978]. It is given by:

$$\Gamma \approx \frac{D^2}{2 \cdot \left(\frac{n_{eff2}}{n_{eff1}}\right)^4 + D^2} \tag{2.8}$$

where

$$D^2 = \left(4\pi^2 \frac{W^2}{\lambda^2}\right)\left(n_{eff2}^2 - n_{eff1}^2\right) \tag{2.9}$$

in which W is the width of the guide. A plot of the results obtained by using the indices of refraction from the effective index method is shown in Fig. 2.4. It can be seen that for ridge widths of less than about 1μm the optical mode is not well confined beneath the ridge. For ridge widths greater than 1.5μm (the smallest size examined), the optical mode is almost completely confined under the ridge.

2.5 INDEX OF REFRACTION OF *InGaAsP*

The material system for the long wavelength semiconductor lasers used in this thesis is $In_{1-x}Ga_xAs_yP_{1-y}$ (with the composition fractions given by x and y) grown on an *InP* substrate. There are several empirical relationships that have been derived to calculate the index of refraction of *InGaAsP*. An equation developed by Suematsu [1982] for the index of *InGaAsP* which is lattice matched to *InP* is:

$$n^2=1+\frac{E_d}{E_o}+\frac{E_d}{E_o^3}E^2+\frac{\eta}{\pi}E^4\ln\left(\frac{2E_o^2-E_g^2-E^2}{E_g^2-E^2}\right) \tag{2.10}$$

where

$$\eta=\frac{\pi E_d}{2E_o^3(E_o^2-E_g^2)} \tag{2.11}$$

$$E_o=3.391-1.652y+0.863y^2-0.123y^3 \tag{2.12}$$

$$E_d=28.91-9.278y+5.626y^2 \tag{2.13}$$

and

$$E_g=1.35-0.72y+0.12y^2 \tag{2.14}$$

These equations are evaluated at a photon energy of $E(=h\nu)$. When the photon energy is close to the band gap, the above equations are not valid. Instead, the phase index of a quaternary extending to infinity can be described by an equation derived by Burkhard [1984]:

$$n(\Delta E,y)=3.425+0.94\Delta E+0.952(\Delta E)^2+(0.255-0.257\Delta E)y-(0.103-0.092\Delta E)y^2$$

The variable ΔE represents the energy separation between the band-gap of the material and the wavelength of the light ($\Delta E=E_g$-E_{ph}). This equation is valid when the photon energy is within 0.2eV of the band-gap (-0.2eV$\leq\Delta E\leq$0eV), which equates to a wavelength of approximately 1.3-1.6μm [Burkhard,1984]. The above equations are used to calculate the index of the barriers and cladding regions which are unstrained. In materials where there is strain (i.e. in the quantum wells) the above equations are not valid. Since the amount of material within the quantum wells is small, it is satisfactory to interpolate linearly between the binary values to find the approximate index. For reference, the binary indices are given in Table 2.1.

Table 2.1: Indices of refraction for the Binary Compounds [Burkhard,1984]

Parameter	*InAs*	*InP*	*GaAs*	*GaP*
Index of Refraction at λ=1.3μm	3.515	3.21	3.338	3.1

CHAPTER 3: LATERAL CURRENT FLOW MODEL

3.1 INTRODUCTION

The behaviour of carriers within semiconductor materials is of interest to laser designers. This is largely because gain can only occur in the region of the laser where there are sufficient numbers of carriers and photons. This region is referred to as the gain or active region. In semiconductor lasers, carriers are injected into the gain region. Any carriers which escape from this region without recombining to produce a photon that contributes to the optical mode are construed as a loss. Spontaneous emission is also considered a loss- especially if it occurs outside the active region. The main loss mechanism of interest in this thesis is the lateral flow out of the active region. In this chapter, simplifying approximations are used to solve the current continuity equations to produce an analytical model. An analytical model was favoured since it is much easier to visualize how the manipulation of the various parameters will affect the model and hence, simplifies the fitting of the model to experimental data.

3.2 ASSUMPTIONS AND APPROXIMATIONS USED IN SOLVING THE CURRENT CONTINUITY EQUATIONS

To calculate the lateral carrier profile and current flow within a semiconductor laser, it is necessary to solve the current continuity equations which describe carrier motion within semiconductors. An analytical solution to these equations was desired since this allows for easy visualization into how adjustments of the various parameters will affect lateral carrier diffusion. To obtain an analytical expression for the lateral current flow, it is necessary to make a variety of assumptions and approximations which will be discussed below.

3.2.1 Current Continuity Equations

The exact solution to the lateral current flow problem in a laser requires the solving of the two-dimensional current continuity equations which would require numerical techniques. One major simplification which enabled the development of an analytical model was the reduction of the problem to one-dimension. This is possible by realizing that the transverse dimensions of the active region are small compared to the lateral dimensions of the device. In such a situation, the time that it takes for the carriers to diffuse across the active region (in the transverse direction) may by assumed to be instantaneous in comparison to the time that it takes for the carriers to diffuse any distance laterally.

The motion of electrons and holes in a semiconductor can be described by differential equations known as the current continuity equations. In one dimension, these are given by:

$$\frac{\partial p}{\partial t}=-\frac{1}{q}\frac{\partial J_p}{\partial x}-\frac{p}{\tau_p}+G \tag{3.1}$$

and

$$\frac{\partial n}{\partial t}=\frac{1}{q}\frac{\partial J_n}{\partial x}-\frac{n}{\tau_n}+G \tag{3.2}$$

In the above equations, n and p refer to the electron and hole densities respectively, J is the current density of the current flowing in the x-direction, τ is the carrier lifetime, and G is the carrier generation rate per unit volume [Wolfe, 1989, p.248]. The current density for electrons flowing in the lateral direction is:

$$J_n=q\mu_n\, n\xi+qD_n\frac{\partial n}{\partial x} \tag{3.3}$$

and for holes:

$$J_p=q\mu_p\, p\xi-qD_p\frac{\partial p}{\partial x} \tag{3.4}$$

In these equations, μ refers to the mobility, D is the diffusion coefficient and ξ refers to the electric field. By combining (3.1) to (3.4) one obtains:

$$\frac{\partial n}{\partial t} = n\cdot\mu_n\frac{\partial \xi}{\partial x} + \mu_n\cdot\xi\frac{\partial n}{\partial x} + D_n\frac{\partial^2 n}{\partial x^2} + G - \frac{n-n_o}{\tau_n}-\frac{J_{n_{in}}}{d\cdot q} \tag{3.5}$$

and

$$\frac{\partial p}{\partial t} = -p\mu_p\frac{\partial \xi}{\partial x} - \mu_p \xi \frac{\partial p}{\partial x} + D_p\frac{\partial^2 p}{\partial x^2} + G - \frac{p-p_o}{\tau_p} + \frac{J_{p_{in}}}{d \cdot q} \tag{3.6}$$

where J_{pin} and J_{nin} refer to the current density of the holes and electrons flowing into the active region (in the z-direction). The notation used is illustrated in Fig. 3.1. In this thesis, we are only concerned with the steady state conditions so that the time derivatives in (3.5) and (3.6) can be considered to be zero which results in:

$$n\mu_n\frac{\partial \xi}{\partial x} + \mu_n \xi \frac{\partial n}{\partial x} + D_n\frac{\partial^2 n}{\partial x^2} + G - \frac{n-n_o}{\tau_n} - \frac{J_{n_{in}}}{d \cdot q} = 0 \tag{3.7}$$

and

$$-p\mu_p\frac{\partial \xi}{\partial x} - \mu_p \xi \frac{\partial p}{\partial x} + D_p\frac{\partial^2 p}{\partial x^2} + G - \frac{p-p_o}{\tau_p} + \frac{J_{p_{in}}}{d \cdot q} = 0 \tag{3.8}$$

An additional assumption needs to be noted at this time. A constant lifetime beneath the ridge is required to simplify the calculations for the development of an analytical solution. In reality, the carrier lifetime depends on both the carrier density and the optical power [Agrawal, 1993, p.57]. Since the carrier distribution and the optical profile drop to zero away from the ridge boundary, it is apparent that the assumption of a constant lifetime is not completely valid. Nevertheless, a constant lifetime is assumed and the validity of this assumption will be discussed further later.

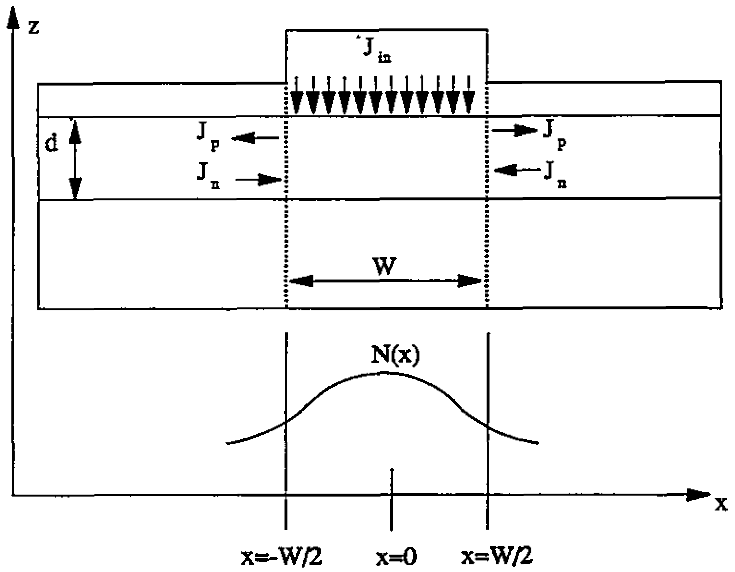

Figure 3.1 Illustration of the nomenclature for the lateral current spreading problem.

3.2.2 Ambipolar Diffusion

It may have been noted that (3.7) and (3.8) contain terms with an electric field component, even though in the lateral direction there is no applied electric field. However, since electrons and holes move at different speeds through the semiconductor (the electrons being faster than the holes), localized electric fields are formed. This effect can be understood by realizing that charge neutrality must be conserved within the semiconductor. In that way, when the carriers move, the faster carrier will drag along the slower carrier [Wolfe, 1989]. The carrier motion is identical to that of diffusion and can be described by an effective diffusion rate known as ambipolar diffusion. The ambipolar diffusion coefficient can be easily derived from the current density equations already presented (equations 3.3 and 3.4). The basis of the ambipolar diffusion approximation is charge neutrality, which requires that the total current flow at each point to be zero (ie. $J_n+J_p=0$). In addition, charge neutrality also requires that $n=p$ and $\partial n/\partial x=\partial p/\partial x$ since the carrier profiles of the electrons and holes must be identical. Using these results, it is possible to rewrite (3.3) and (3.4) as:

$$J_n=qD_a\frac{\partial n}{\partial x} \tag{3.9}$$

and

$$J_p=-qD_a\frac{\partial p}{\partial x} \tag{3.10}$$

where D_a is defined as the ambipolar diffusion coefficient and is given by:

$$D_a=\frac{\dfrac{D_p}{\mu_p}+\dfrac{D_n}{\mu_n}}{\dfrac{1}{\mu_p}+\dfrac{1}{\mu_n}} \tag{3.11}$$

The derivation of this equations is described in detail in Appendix I. Using this result, (3.7) and (3.8) are rewritten as:

$$D_a\frac{\partial^2 n}{\partial x^2}+G-\frac{n}{\tau_n}-\frac{J_{n_{in}}}{d\cdot q}=0 \tag{3.12}$$

and

$$D_a\frac{\partial^2 p}{\partial x^2}+G-\frac{p-p_o}{\tau_p}+\frac{J_{p_{in}}}{d\cdot q}=0 \tag{3.13}$$

For a ridge type device with the ridge being p-doped and the bottom layer being made of a relatively conductive n-doped material (which is the same as that found in a ridge waveguide laser), Joyce [1982] also proposed a model which is equivalent to the ambipolar diffusion model when $\mu_n >> \mu_p$. In the model, the injection of the holes is limited to the active region due to the width of the ridge. This means that the carrier distribution is determined by the lateral diffusion of holes out of the active region. The n-doped region beneath the active region provides a broad area contact to the active region so the electrons can be injected into the active region at any location along the width of the laser to maintain charge neutrality within the active region. Therefore, the effect of electrons on the current spreading is neglected since the distance that they must diffuse within the active region is much less than that of the holes. In other words, electrons are supplied from the n-layer to provide charge neutrality but are, to a first approximation, stationary within the active region [Joyce, 1982]. This means that the current spreading is essentially described by the lateral drift and diffusion of the holes, resulting in an effective diffusion rate describe by the equation [Joyce, 1982]:

$$D_{eff} = \mu_p \left(\frac{D_p}{\mu_p} + \frac{D_n}{\mu_n} \right) \tag{3.14}$$

This expression is equivalent to (3.11) whenever $\mu_n >> \mu_p$.

By using the ambipolar diffusion approximation and the fact that the number of holes equals the number of electrons, it is possible to combine the current continuity equations and talk simply about the sum of the carrier densities ($N=n+p$). Instead of investigating the numbers of holes and electrons being injected into the active region separately, the total number of carriers being injected is considered. To this end, equations (3.12) and (3.13) are simply added together. It must also be noted that the hole lifetime equals the electron lifetime, and that the total current density is defined as $J_{pin}-J_{nin}=J_{in}$. The new equation is:

$$D_a \frac{\partial^2 N(x)}{\partial x^2} + \frac{J_{in}}{d \cdot q} - \frac{N(x)}{\tau} = 0 \tag{3.15}$$

where *N(x)* is the carrier density profile. The number of injected carriers is assumed to be constant beneath the ridge and zero elsewhere. The carrier generation rate was assumed to be negligible since the laser is forward biased.

3.3 LATERAL CURRENT FLOW SOLUTIONS

The linear second-order differential equation (3.15) can be solved by realizing that the charge profile must be continuous and smooth at the ridge boundary. This results in the requirement that the carrier profile and its derivative must be constant across the ridge boundary. The other requirement is that the carrier density approaches zero as x approaches infinity. J_{in} is assumed to be constant beneath the ridge, and zero elsewhere. These conditions yield an expression for the carrier density profile outside the ridge given by:

$$N(x) = \frac{J_{in} \cdot \tau}{q \cdot d} e^{-|x|/L_D} \cdot \sinh\left(\frac{W}{2L_D}\right) \qquad |x| > \frac{W}{2} \tag{3.16}$$

and beneath the ridge given by:

$$N(x) = \frac{J_{in} \cdot \tau}{d \cdot q} \cdot \left(1 - e^{-W/2L_D} \cdot \cosh\left(\frac{x}{L_D}\right)\right) \qquad |x| < \frac{W}{2} \tag{3.17}$$

where W is the width of the ridge and L_D is the diffusion length. The diffusion length is defined as $L_D=(D_a\tau)^{1/2}$ and it represents the average distance that a carrier will diffuse before it recombines.

It is useful to define a term, J', which represents the average recombination current density beneath the ridge:

$$J' = \frac{d \cdot q}{W} \cdot \int_{-\frac{W}{2}}^{\frac{W}{2}} \frac{N(x)}{\tau} dx \tag{3.18}$$

which is simply the total number of carriers beneath the ridge divided by their average lifetime beneath the ridge. Evaluating (3.18), one obtains:

$$J' = J_{in} \left[1 - \frac{L_D}{W}\left(1 - e^{(-W/L_D)}\right)\right] \tag{3.19}$$

This can be related to the input current of the laser by realizing that

$$I_{in}=J_{in}\cdot L_c\cdot W \tag{3.20}$$

where L_c is the length of the device. Transposing (3.19) yields:

$$I_{in} = \frac{J'\cdot L_c\cdot W}{1-\frac{L_D}{W}\left(1-e^{-W/L_D}\right)} \tag{3.21}$$

which is an expression for the input current as a function of the ridge width, J' and L_D.

It is interesting to note that the injection current can be written as the sum of the recombination current beneath the ridge and the lateral current flow:

$$I_{in}(W)=J'\cdot L_c\cdot W+I_L(W) \tag{3.22}$$

where the variable I_L is defined as the lateral current. By substituting (3.21) into (3.22), one can obtain an expression for the lateral current flow:

$$I_L(W) = \frac{J'\cdot L_c\cdot L_D\left(1-e^{-W/L_D}\right)}{1 - \frac{L_D}{W}\left(1-e^{-W/L_D}\right)} \tag{3.23}$$

These last two equations show that for $W \gg L_D$, this function reduces to a linear equation with the lateral current being a constant equalling $J'\cdot L_c\cdot L_D$.

In the above derivation, the carrier lifetime was assumed to be constant throughout the laser structure. Since the lifetime depends on both the carrier density and the photon density within the laser, a more accurate model would be to assume two different lifetimes: one beneath the ridge and one outside the ridge boundary. If this is assumed to be the case, the expression for I_L would become:

$$I_L = J'L \frac{2L_{D1}^2 \sinh\left(\frac{W}{2L_{D1}}\right)}{L_{D1}\cosh\left(\frac{W}{2L_{D1}}\right) + L_{D2}\sinh\left(\frac{W}{2L_{D1}}\right) - 2\frac{L_{D1}^2}{W}\sinh\left(\frac{W}{2L_{D1}}\right)} \tag{3.24}$$

where L_{D1} is the diffusion length beneath the ridge and L_{D2} is the diffusion length outside the ridge. This expression is derived in detail in Appendix II. The main difficulty with applying this equation to experimental data is that there is an additional degree of freedom and different combinations of L_{D1} and L_{D2} produce approximately the same value for I_L, which results in some ambiguity in the equation. This makes it difficult to use (3.24) to fit varying ridge width data and obtain a meaningful result. This is discussed further in the next chapter.

3.4 ILLUSTRATIONS OF THE MODEL

This section contains illustrations of some of the features of the model which was developed in the previous section. Also discussed are some of the limitations of the model.

3.4.1 Carrier Profiles and Current Flow

It is possible to calculate the carrier profile from (3.16) and (3.17) and compare the profiles obtained for the different ridge widths by assuming a diffusion length of 1μm

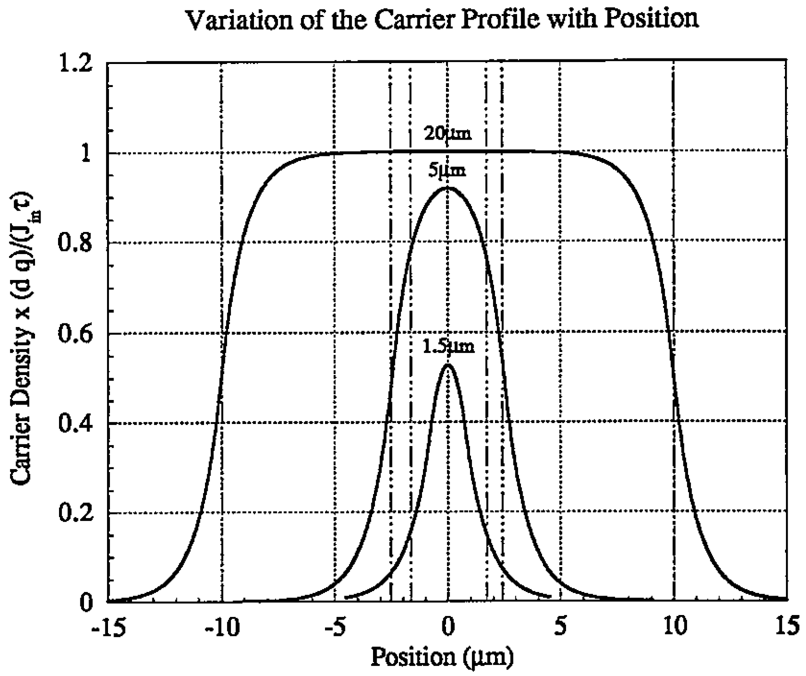

Fig. 3.2 Plot of the carrier profile for ridge widths of 1.5, 5, and 20μm and a diffusion length of 1μm.

(which will be shown in Chapter 4 to be a typical value for the lasers investigated) and by normalizing the equation by setting the factor $(J_{in} \cdot \tau/(q \cdot d))$ to unity (for ease of illustration). The carrier profile results are illustrated in Fig. 3.2 from which we see that the fraction of carriers outside the ridge boundary decreases with increasing ridge width. This results in the larger ridge widths being more efficient with a smaller current per unit ridge width having to be applied to obtain a specified operating point.

Often in calculations, for example to estimate the threshold current of a laser, the gain and the optical power are assumed to be constant across the width of the active region. However, the carrier density is not constant, so it is evident that the gain (which varies with the carrier density) will also not be constant across the lateral profile of the laser. From simple waveguide theory, it is evident that the optical power profile is not constant either. If the gain is assumed to be proportional to the carrier density, it would be more accurate to consider the overlap of the optical mode and the carrier profile. The reasoning for this is as follows: since threshold is defined as the point where the round trip gain equals the round trip losses (minus the contribution of spontaneous emission), the gain of the optical mode for each of the ridge widths should be identical at threshold. This suggests that the overlap should be identical for all the different ridge widths at threshold. This will be discussed further in Section 4.5.

It was previously mentioned that the carrier lifetime is not constant- especially as one moves away from the boundary where the carrier concentration approaches zero. For illustration purposes, the calculations shown here are based on a single carrier lifetime since it is easier to visualize what is happening when there are fewer parameters to manipulate. The actual carrier density profile will be somewhat distorted from what is shown here. Even so, the slope of the profile at the ridge boundary multiplied by the diffusion coefficient will be approximately constant for the two methods since the slope determines the lateral current, and, as will be shown later, the amount of lateral current calculated by both methods is nearly identical. Absolute magnitudes of the lateral currents are also of interest. As can be seen from Fig. 3.3, the lateral current is a strong function of ridge width for small ridge widths (<5μm). When L_D=1.5μm, and $J'L_c$=1.9mA/μm (which are values obtained in Section 4.5), it can be seen that as much as 60% of the current escapes out of the active region for the smaller ridge widths. It is also useful to plot the fraction of current lost to the gain of the optical mode due to lateral current flow as a function of ridge width. The fraction of current flowing outside the ridge for L_D equalling 0.3µm and 1.6µm (the values obtained for temperatures of +60°C and -40°C at threshold in Section 4.4) is illustrated in Fig. 3.4. As can be seen, the fraction of current escaping out of the active region decreases with a decreasing diffusion length.

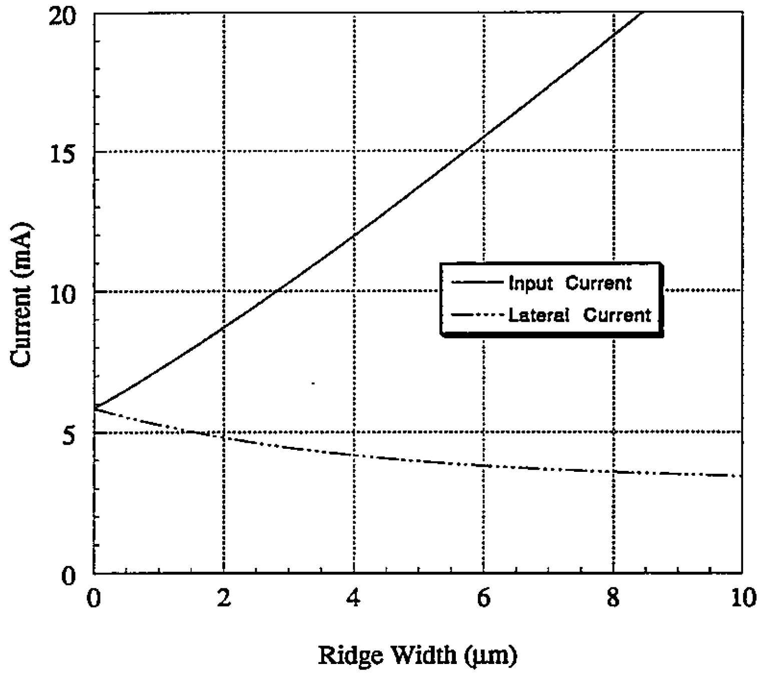

Fig. 3.3 The calculated variation of leakage current with ridge width for $J' \cdot L_c$=1.9mA/µm, L_D=1.5µm.

3.4.2 Limitations of the Model

There are several limitations to this model that must be noted. Most importantly, the above discussion is only valid for situations where the optical confinement is approximately unity so there is a definite, measurable boundary between the regions of gain and loss. If the optical mode is well confined to the region beneath the ridge then

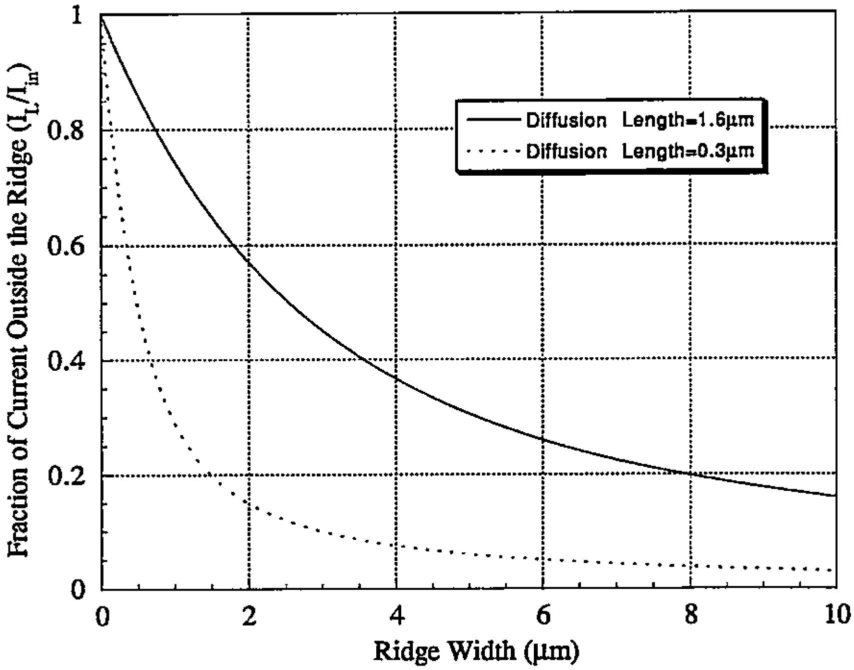

Fig. 3.4 The fraction of current escaping from under the ridge as a function of ridge width for L_D=0.3µm and L_D=1.6µm.

only the carriers beneath the ridge will contribute to its gain. This means that the boundary which marks the separation between those carriers which contribute to gain and those which are lost is equivalent to the ridge boundary. If the optical mode was not well confined, it would be necessary to define and then calculate an effective ridge width which corresponds to the width of the gain region. Otherwise, the boundary of the active region will not be equivalent to the boundary of the ridge, and the lateral current flow will be overestimated. This will be investigated further later (in Section 4.5) by considering the overlap of the optical mode with the carrier profile. Also, to compare the lasers directly, a common operating point must be considered. Possible operating points are discussed in Section 4.4.

There are two other details that are important to note: it is assumed that the magnitude of internal heating does not change with changing ridge width, and that the lasers are in single-mode operation for all ridge widths. The requirement for single mode operation will also be discussed further in Section 4.5.

CHAPTER 4: EXPERIMENTAL APPARATUS, PROCEDURES AND RESULTS

4.1 INTRODUCTION

The focus of this chapter is on the application of the previously derived model to the interpretation of the experimental data. The first part of this chapter describes the experimental apparatus and procedures. This is followed by the L-I curves measured from lasers of different ridge widths and the application of the model to the raw data. The final section examines the validity of the assumptions used to form the model.

4.2 LASER STRUCTURE

The structure investigated here consists of a strained-layer multiple-quantum well (MQW) ridge waveguide laser constructed in the *InGaAsP-InP* material system. As illustrated in Fig. 4.1, the strain in the quantum wells was alternated between compressive and tensile. This reason for the unusual structure is because the laser was constructed on a wafer which was grown for an amplifier that was designed to be polarization insensitive. A total of 40 devices with ridge widths of the waveguide varying from 1.5μm to 100μm, with ridge heights of 1.5μm were studied. Four devices of each ridge width were investigated to minimize the error incurred due to abnormal devices. Ten

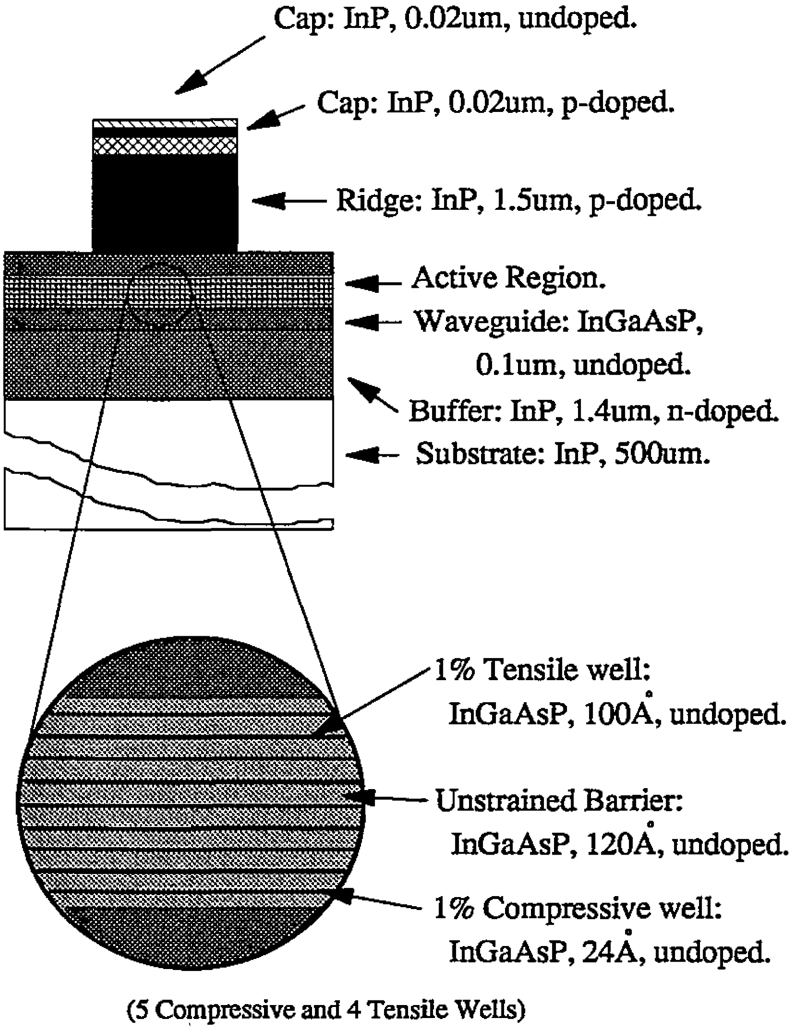

Fig. 4.1: Illustration of the quantum well structure investigated.

different ridge widths were examined in total. However, the investigation was limited to the seven sets of lasers with ridge widths equal to or less than 5μm since noticeable deviations occur for the larger ridge widths. (The threshold currents were larger than expected.) This may be attributed to the fact that for ridge widths of more than 5μm, the device no longer operates in the first optical mode, and to additional internal heating arising from the increased ridge size.

After fabrication, the lasers were mounted as illustrated in Fig. 4.2. This allowed for easy connection into the experimental apparatus without damage to the laser.

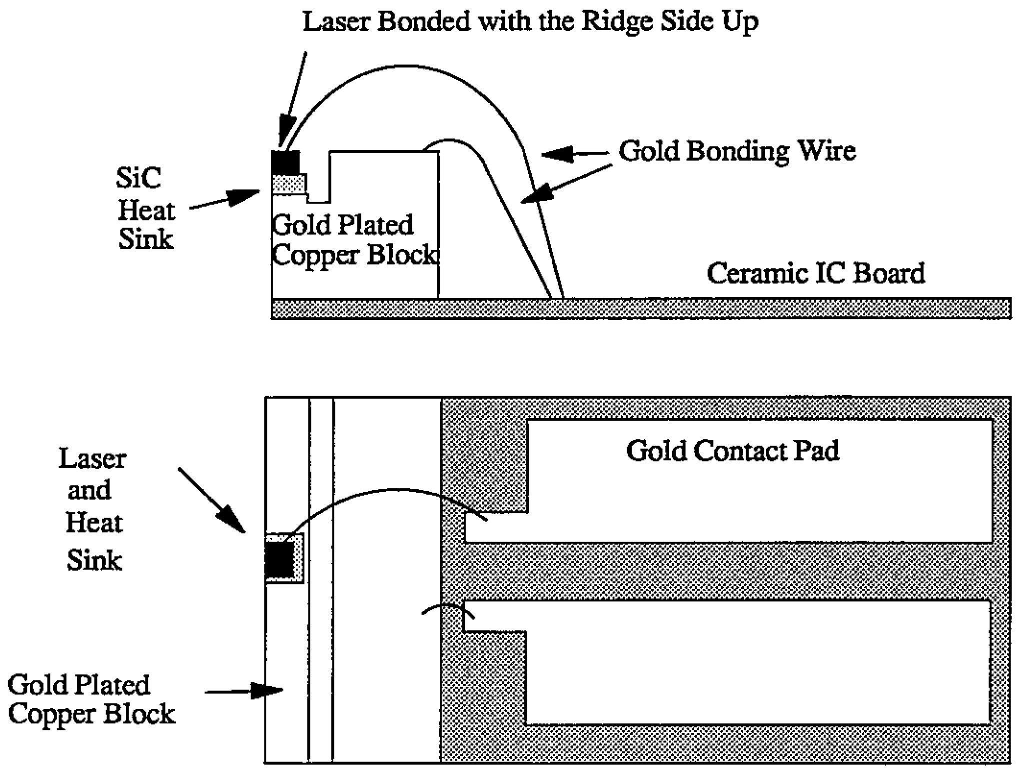

Fig. 4.2 Diagram illustrating the laser mount.

4.3 EXPERIMENTAL APPARATUS AND PROCEDURES

The experimental apparatus in this thesis was designed to measure the L-I curves of semiconductor lasers as a function of temperature. This section gives a description of the apparatus and some of the procedures used to obtain consistent results between the devices.

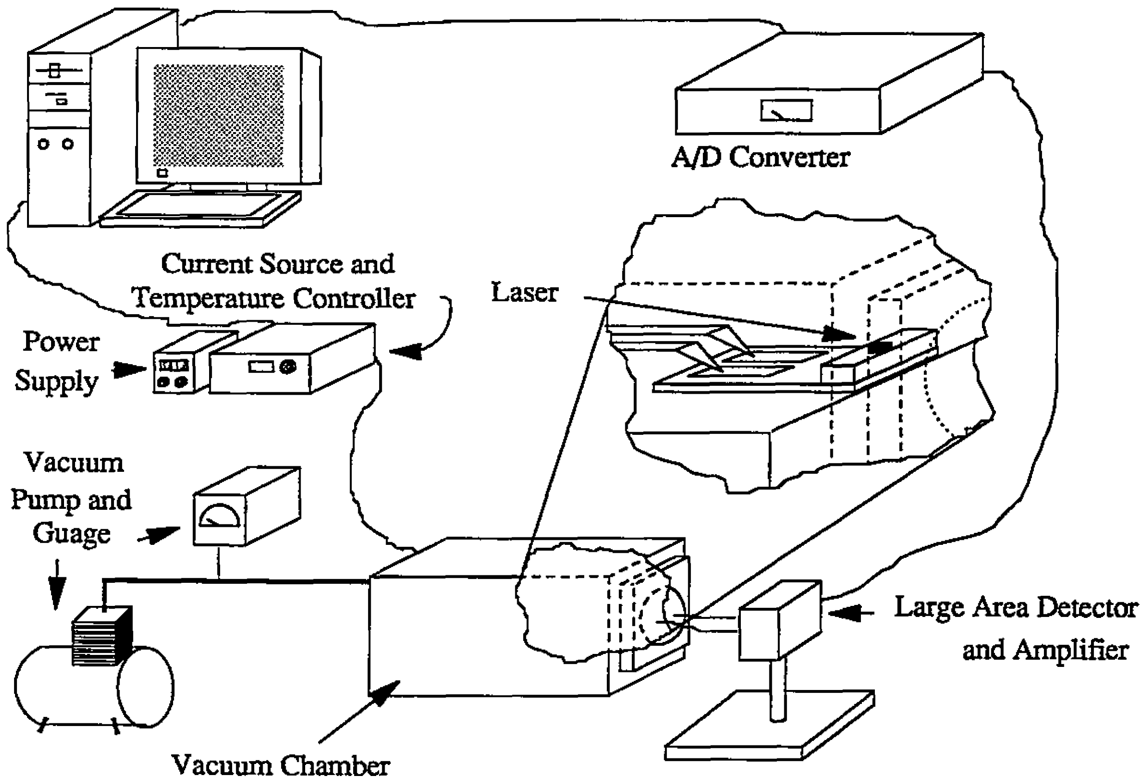

Fig. 4.3: Experimental apparatus to measure the CW output of semiconductor lasers as a function of current and temperature.

The apparatus for measuring the continuous wave (CW) light output as a function of both current and temperature is shown in Fig. 4.3. The laser is placed on a copper mount within the vacuum chamber. The mount is temperature stabilized by using a two-stage water-cooled thermoelectric cooler. The vacuum is required to minimize both the amount of condensation on the laser at lower temperatures and the distortion of the output of the laser by the absorption lines of water. Both the temperature and the laser current are controlled by the ILX 3722 Laser Current Source (LCS). The output is collected by the large area, $1cm^2$, calibrated germanium detector, which is then amplified 2000 times by a transimpedence (current-to-voltage) amplifier. The signal is then digitized by using the analog-to-digital converter incorporated in a SR510 lock-in amplifier. The data acquisition is accomplished by a PC which is interfaced to the lock-in amplifier and the LCS by a GPIB card.

The measurement process itself is computer controlled. During the measurement, the base temperature is stabilized to the set temperature to within 0.2°C and held at that temperature for a least 1 minute before the measurement is taken. There is currently no correction for the temperature difference expected to exist between the base temperature and the active region temperature. The collected data was corrected for the wavelength dependence of the sensitivity of the detector by measuring the peak wavelength at temperatures ranging from 20°C to 90°C. The emission wavelengths at lower temperatures were obtained by a linear extrapolation of these values. The detector is relatively insensitive to wavelength changes in the range investigated, so the linear extrapolation should be valid.

4.4 EXPERIMENTAL RESULTS

4.4.1 Data Collection

A sample of the light versus current (L-I) characteristics is shown in Fig. 4.4. These curves were corrected for the wavelength response of the detector, and were obtained at a laser base temperature of -40°C. Specific operating points were selected from these curves. The data was then extracted for further analysis.

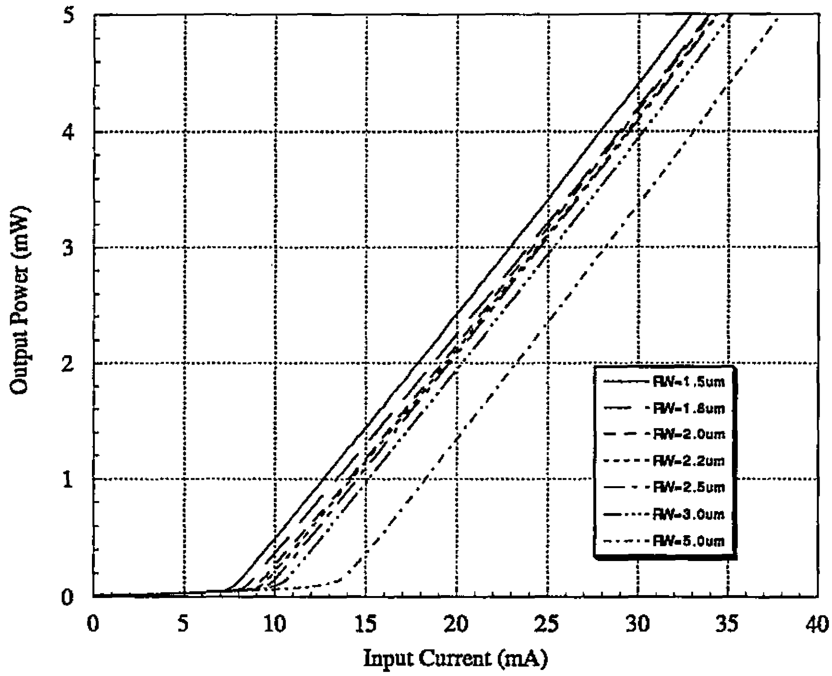

Fig. 4.4 The L-I characteristics for lasers of different ridge widths at -40°C.

4.4.2 Data Evaluation

In this section, the model derived in Section 3.3 is applied to the L-I curves from the laser structure on hand. An inspection of (3.21) shows that by plotting the input current required to reach a specific operating point on the L-I curve as a function of the ridge width, it is possible to obtain J' and L_D. This can be accomplished by fitting the equation to the varying ridge width data by using the method of least squares.

To be able to compare the currents injected into the lasers of different ridge widths, an operating point which is common to all the different ridge widths is required.

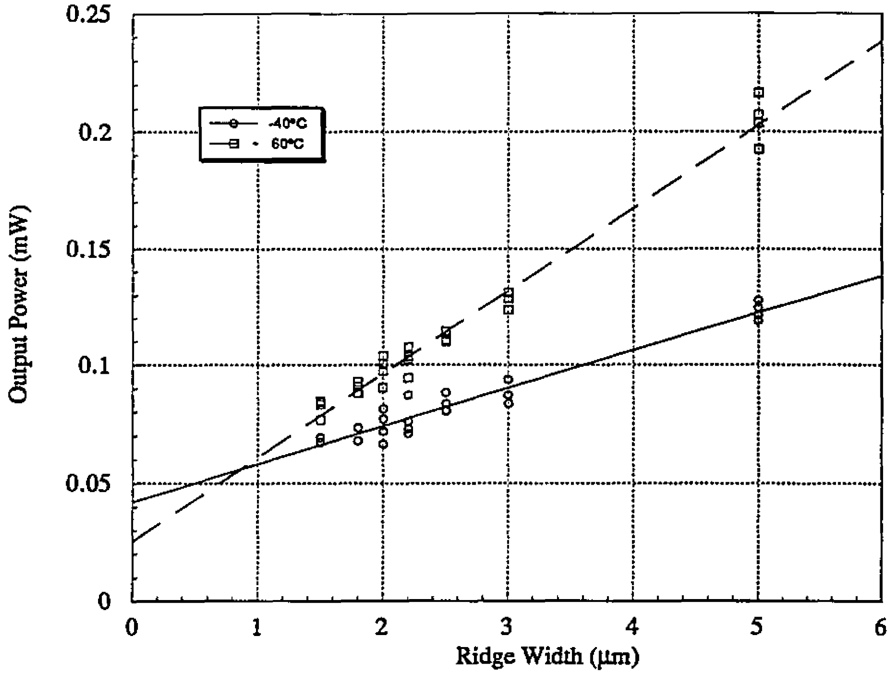

Fig. 4.5 Variation of the output power at threshold with ridge width at different temperatures.

For this investigation, threshold and a constant power per unit ridge width were chosen for the analysis. It must be assumed that the escaping carriers do not contribute significantly to the optical mode, and hence, the output power levels chosen must be large enough that the spontaneous emission emitted from the lateral current outside the active region is negligible. The amount of spontaneous emission contributed by this lateral current can be determined by plotting the variation of the output power at threshold versus the ridge width as shown in Fig. 4.5. The maximum optical power contributed to the output by the lateral current was found to be approximately 0.04mW at threshold.

To minimize the effect of the spontaneous emission from the lateral current, large output power levels were chosen: 0.25mW to 1mW per unit ridge width. These are significantly greater than the 0.04mW of optical power contributed by the lateral current flow. It was realized that the lateral current will change with pumping which will, in turn, increase the spontaneous emission occurring outside the active region; however, it is assumed that the optical power collected from the spontaneous emission remains negligible as compared to the output power from the optical mode. This is supported by the fact that when the pumping level is changed from the threshold condition to one which produces 0.25mW per unit ridge width, the lateral current changes only slightly. As well, only a small fraction of spontaneous emission emitted from I_L reaches the detector since spontaneous emission is emitted in all directions. Further, if this approximation was not valid, there would be a bowing present in the input current versus ridge width curves. This is because the light emitted from the lateral leakage current divided by the ridge width is not a constant with respect to ridge width.

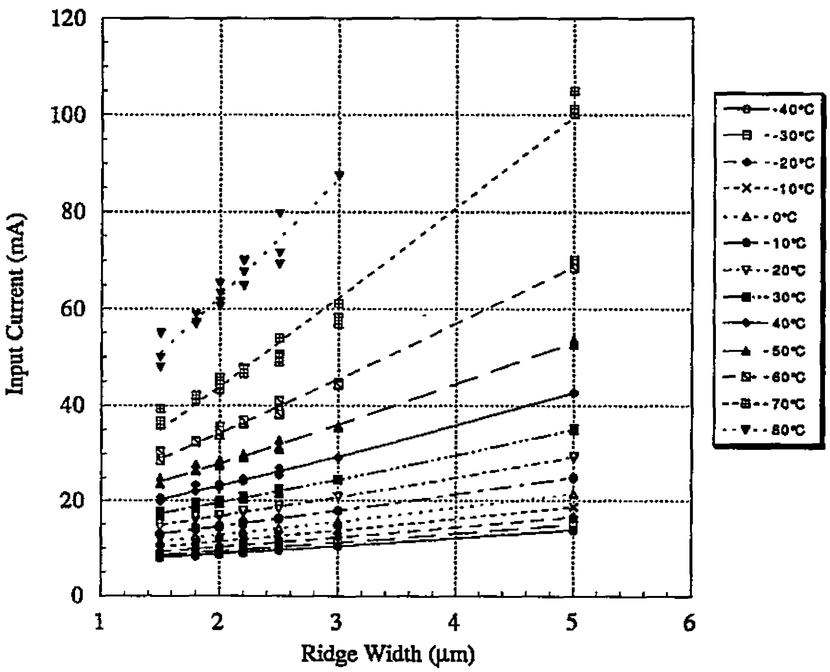

Fig. 4.6 Input current at threshold versus ridge width, with temperature as a parametric variable.

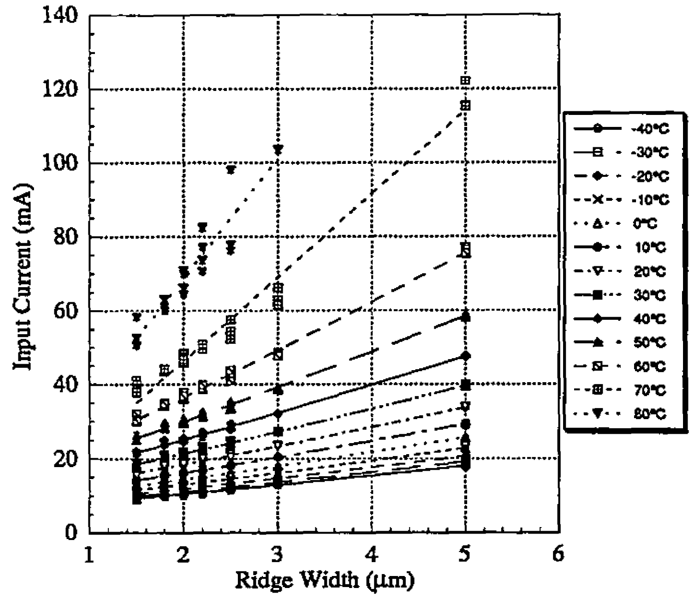

Fig. 4.7 Variation of Current Required to obtain output levels of 0.25mW per micron ridge width as a function of ridge width.

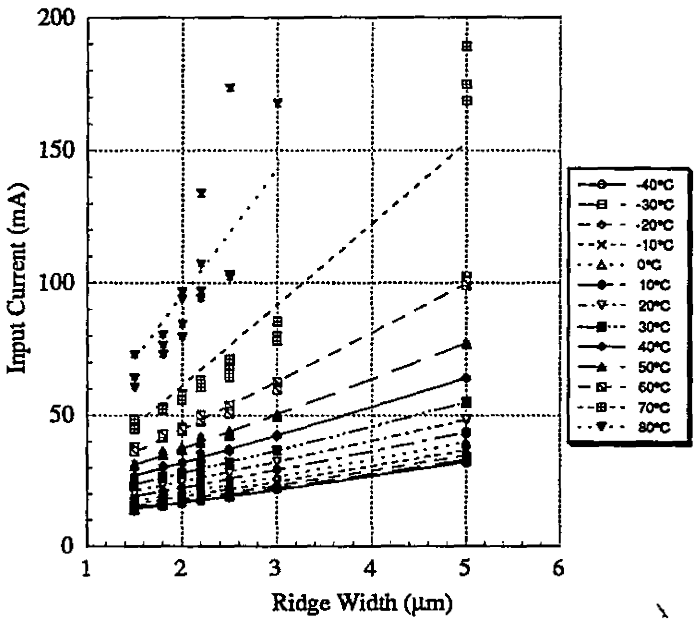

Fig. 4.8 Current Required to obtain output levels of 1.0mW per micron ridge width as a function of ridge width.

Figures 4.6 to 4.8 illustrate the input currents required to reach a specified operating point as a function of ridge width. From these curves, J' and L_D as a function of both pumping power and temperature were obtained by fitting (3.21) to the data by using the method of least squares. The results are shown in Figs. 4.9 and 4.10 respectively. (Note that the investigation from this point is limited to temperatures less than 70°C since above this temperature there is a noticeable deviation, probably due to internal heating, which is not included in the simplified theory used here.) The J' versus ridge width plot is illustrated in Fig. 4.9, and from this plot it is seen that the current density increases with both pumping power and temperature. For each of the pumping powers, the curve is super-exponential with temperature. The reason for this curvature is not understood at this time, but is probably a complicated function of the internal optical loss and carrier loss mechanisms.

Figure 4.10 illustrates how L_D varies with both temperature and pumping power. As one would expect, the diffusion length decreases both with increasing temperature and pumping power. This is because the diffusion length is proportional to $\tau^{1/2}$. This carrier lifetime is in part inversely proportional to the stimulated photon density. As well, an increase in non-radiative processes with temperature (such as Auger recombination) would cause a decrease in the non-radiative carrier lifetime.

The preceding discussion could have used (3.24) (the two lifetime equation) to calculate the lateral current flowing within the device. By applying (3.24) to the data by using a three parameter fit, it was found that the values obtained for J', and hence, I_L

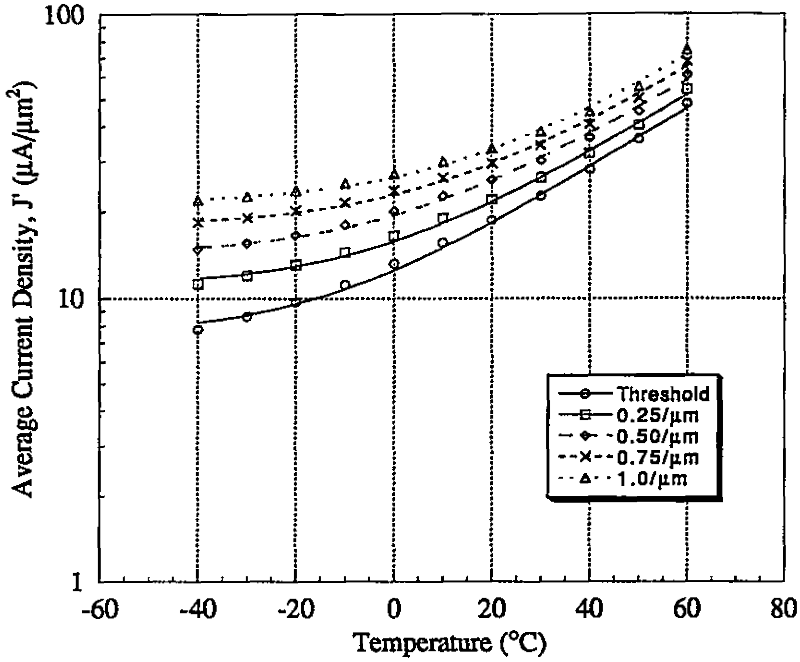

Fig. 4.9 Variation of the average current density under the ridge with temperature and pumping.

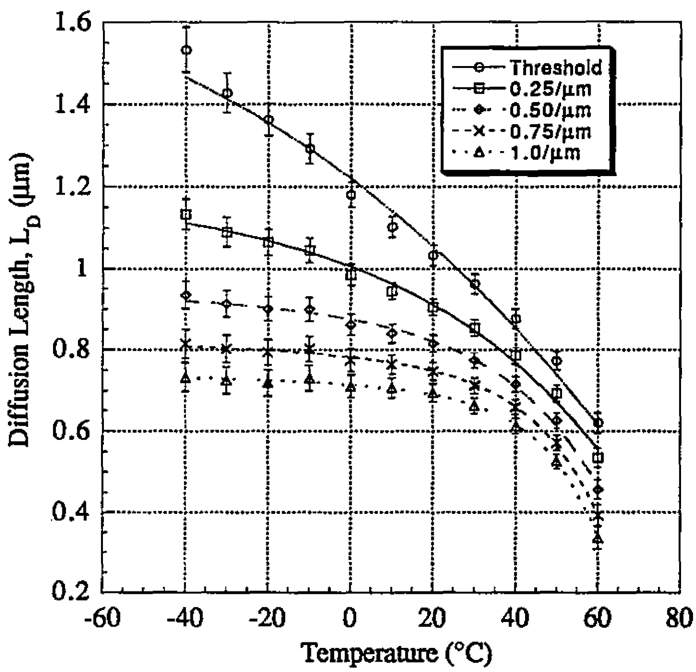

Fig. 4.10 Variation of the diffusion length with temperature and pumping.

($=I_{in}-J''W'L_c$) are identical within error (within 0.8μA/μm^2) to the values obtained by using (3.23). However, this fit yields values of L_{D1} and L_{D2} which have large uncertainties due to the extra degree of freedom. Instead, (3.23) was the chosen expression for the least square fitting of the data due to the fewer degrees of freedom. The motivation behind this is as already mentioned: it provides just an accurate estimate of I_L as (3.24) and I_L is the main parameter of interest in this thesis.

4.5 OVERLAP OF THE CARRIER AND OPTICAL MODE PROFILE

The model, as previous derived, assumes that the overlap between the optical mode and the carrier distribution is constant for each of the ridge widths. Now that values for J' and L_D have been acquired, it is possible to calculate this overlap and check this assumption.

There are two characteristics that can change and will affect the overlap function. The first is the shape of the optical mode. This depends on the effective refractive index of the materials, the width of the ridge, and which mode is propagating. Alternatively, the carrier profile can also change, which is determined by the ridge width and the diffusion length beneath the ridge, the latter varying with temperature and pumping power but being independent of ridge width.

It is a relatively simple process to calculate the overlap of the lateral optical mode and the carrier distribution. The lateral optical power distribution is calculated by assuming a three-layer slab waveguide, as discussed earlier in Section 2.4. The other

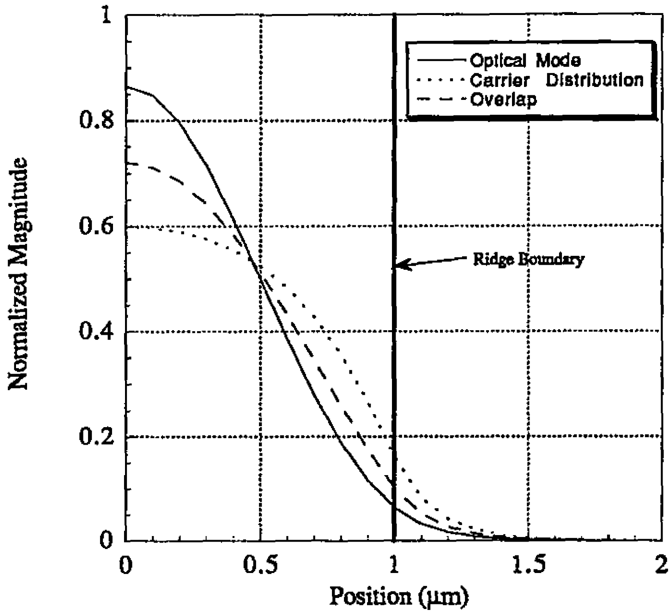

Fig. 4.11 Illustration of the optical mode, carrier distribution and overlap for a 2μm ridge and a diffusion length of 0.3μm.

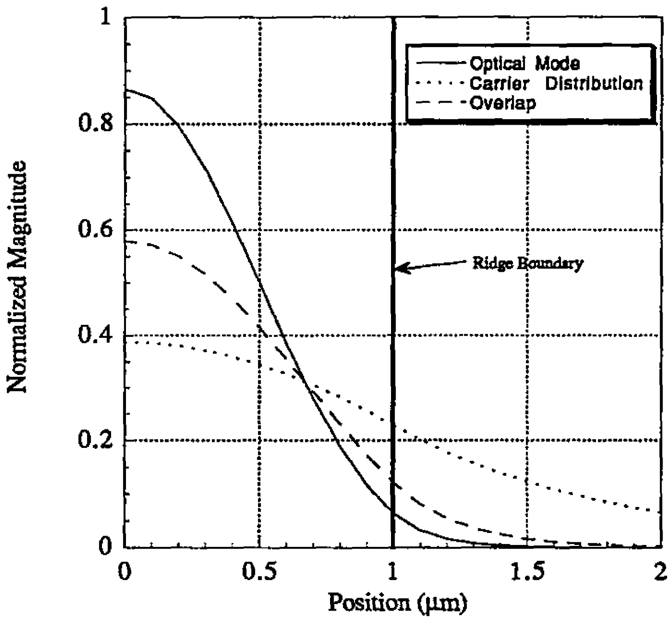

Fig. 4.12 Illustration of the optical mode, carrier distribution and overlap for a 2μm ridge and a diffusion length of 1.6μm.

necessary function, the carrier distribution, is calculated from (3.16) and (3.17). The optical mode, carrier distribution, and the final overlap for a 2μm ridge for two different diffusion lengths were calculated, and the results are illustrated in Figs. 4.11 and 4.12. Each of the functions was normalized to an area of unity beneath the curve. As can be seen here, the carrier profile (which varies with changing diffusion length and ridge width) has a large influence on the final overlap integral. Plots showing the effects of changing ridge width on the overlap for two different diffusion lengths are illustrated in Figs. 4.13 and 4.14. One would expect the dominant mode to be the one with the greatest overlap since there will be the largest interaction between the optical mode and the carriers. For the ridge widths being examined (≤5μm) the dominant mode is the first-order mode for both diffusion lengths. The diffusion lengths chosen represent the extremes of the values obtained from the investigation.

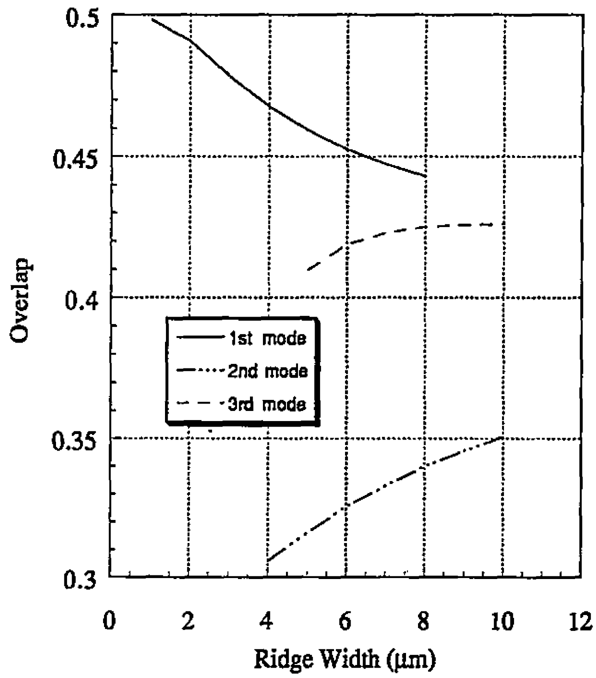

Fig. 4.13 Variation of the overlap with changing ridge width for a diffusion length of 0.3μm.

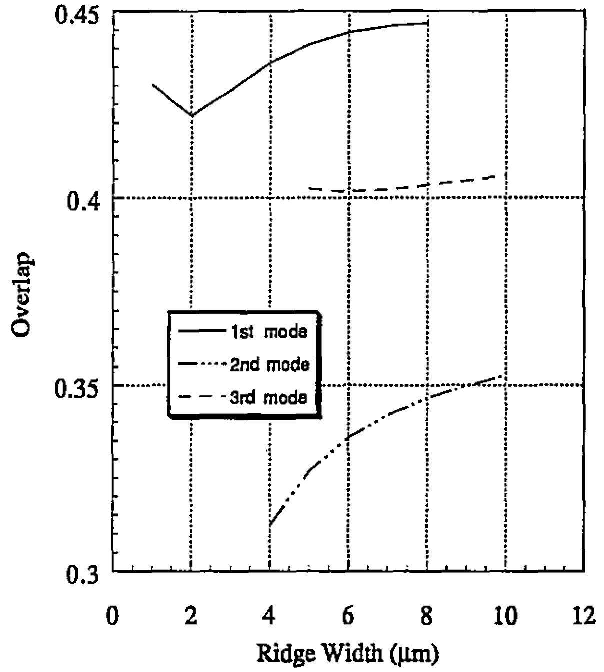

Fig. 4.14 Variation of the mode and carrier overlap for a diffusion length of 1.6μm.

CHAPTER 5: ABOVE THRESHOLD EVALUATION

5.1 INTRODUCTION

The extraction of the average current density (J') and the diffusion length (L_D) from the raw L-I data allows for additional analysis. By using these values, the lateral current can be calculated, from which the effect of lateral current on the output characteristics of the laser (i.e. the external efficiency) can be examined. Also, by manipulating the average current density beneath the ridge and the diffusion length, the linear relationship between J' and τ^{-1} can be investigated. The focus of this chapter is on these additional loss mechanisms.

5.2 EFFECT OF LATERAL CURRENT ON EXTERNAL EFFICIENCY

It is interesting to examine how the lateral current will affect the efficiency of the laser. As already mentioned in Section 3.4, a large fraction of the injected current at threshold (as much as 60%) is lost due to lateral current spreading. This means that the *total* external efficiency (number of photons out/number of carriers in) will be largely affected by this phenomenon as discussed in Section 1.3.2. The effect on the external *differential* efficiency is a little more subtle. If I_L does not change with pumping, it will not have an effect on the differential efficiency. If I_L changes with pumping, there is only one way that it can vary and still allow for a linear L-I curve: it must vary linearly. However, I_L can be either linearly increasing or linear decreasing. Figure 5.1 is a schematic diagram illustrating L-I curves for three different situations: linearly increasing I_L, linearly decreasing I_L, and constant I_L. This illustrates a way that the contribution of I_L can be used to improve the differential of the efficiency- a result which is somewhat counter-intuitive since one usually expects the removal of loss mechanisms to improve the laser characteristics.

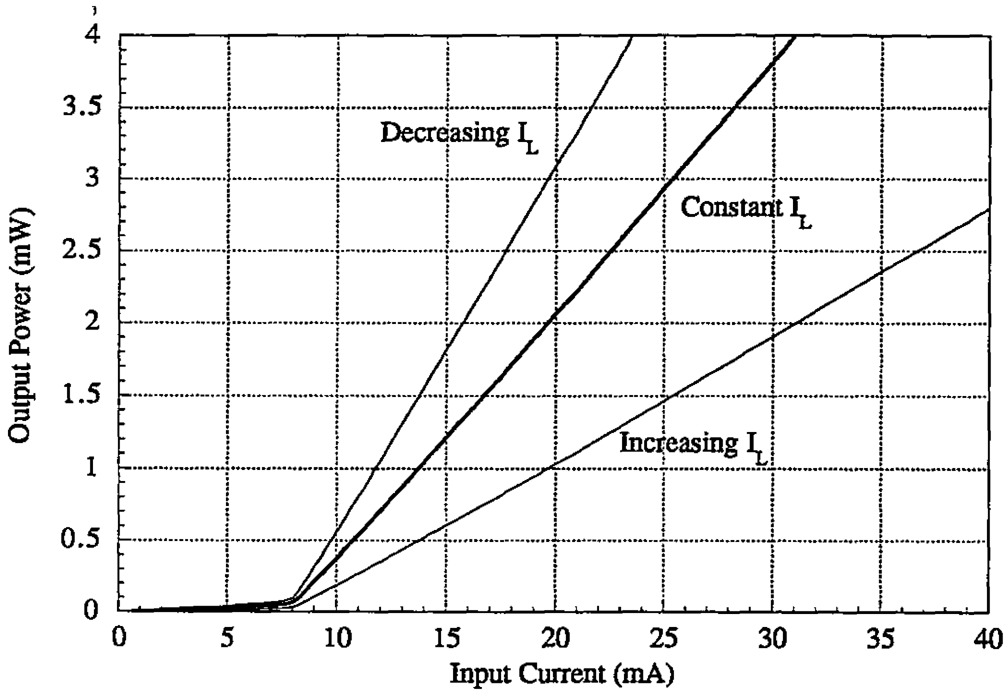

Fig. 5.1 Illustration of the L-I curves for I_L equalling $0.5(I_{in}-I_{th})$, 0, and $-0.5(I_{in}-I_{th})$.

The fraction of the current flowing out of the active region can be expressed by transposing (3.22):

$$\frac{I_L}{I_{in}} = 1 - \frac{J' \cdot W \cdot L}{I_{in}} \tag{5.1}$$

which is a complicated function of L_D, J', and the carrier injection rate (which is essentially I_{in}). Above threshold, the carrier lifetime beneath the ridge will decrease with increased pumping due to the fact that the rate of the stimulated recombination increases. Since the diffusion length decreases, the fraction of the carriers escaping out of the active region will also decrease with pumping. On the other hand, the carrier injection rate is increasing with increased pumping. This has the effect of increasing the number of carriers found outside the active region. This suggests that the lateral current flow will have an effect on the external differential efficiency, but it will not be a simple relationship since there are two different competing factors: the changing lifetime and the changing carrier injection rate. It is of interest to laser designers to calculate what the intrinsic differential efficiency (differential efficiency without lateral current effects) would be.

5.2.1 Internal Efficiency Calculated from the Model

By using the average current density for different pumping levels, it was possible to calculate an I_L-free L-I curve from which the intrinsic differential efficiency (η_d') was calculated. Figure 5.2 is an illustration of L-I curves at two different temperatures both with and without lateral current flow. By close investigation of the curves, it can be seen that when the L-I curves of the intrinsic and measured cases are compared, they diverge

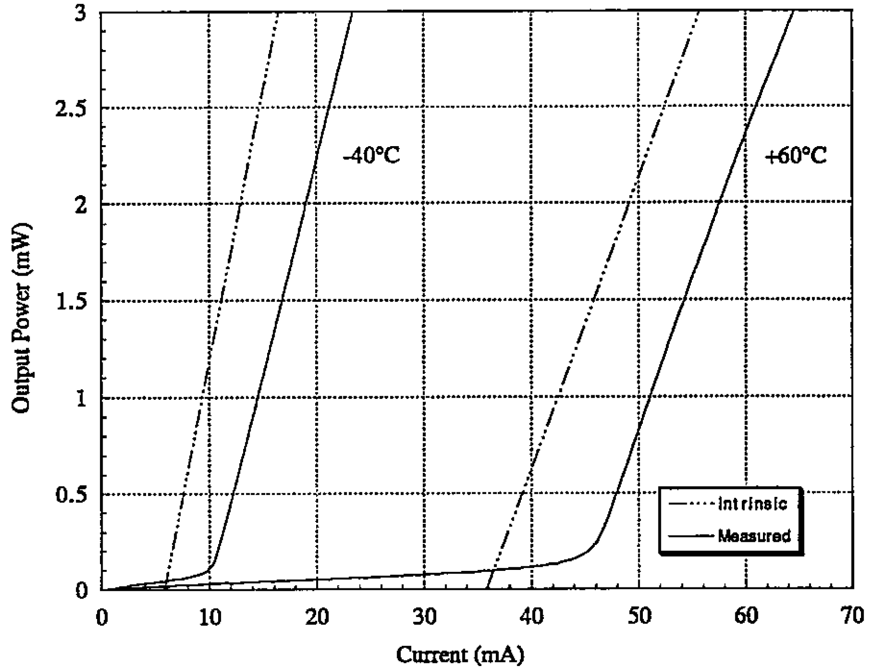

Fig. 5.2 L-I curves both with and without lateral current at -40°C and 60°C for a device with a 3μm ridge.

at -40°C and converge for +60°C. It is therefore evident that I_L has an effect on the differential efficiency which changes with temperature: the contribution of I_L causes a decrease in the efficiency at -40°C, but causes an increase in η_d at +60°C. This is further illustrated by Fig. 5.3, which is a plot of the differential efficiency over the same temperature range, both with and without the lateral current. From the plot it can be clearly seen that there is a crossover point at approximately +45°C which is the point where the lateral current changes from increasing with pumping to decreasing with pumping. This is further illustrated in Fig. 5.4, which is the lateral current flow for a 2μm ridge calculated from the experimentally obtained values of J' and L_D. From this plot it can be seen that at low temperatures, the lateral current increases with pumping, while above +45°C, the opposite is true; hence η_d decreases at low temperatures and

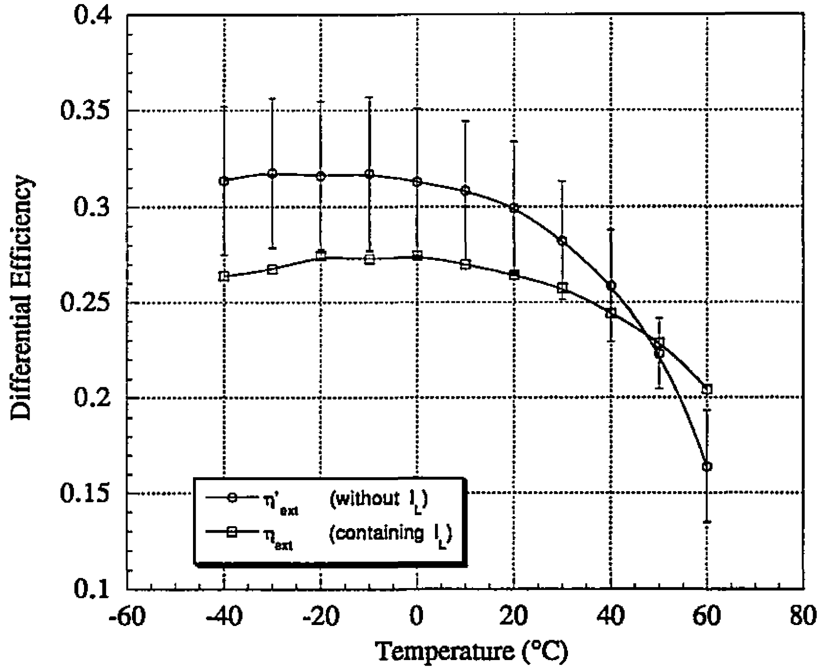

Fig. 5.3 The single facet external differential efficiency shown both with and without lateral current spreading for a 2μm ridge width.

increases it at high temperatures. One can conclude from this analysis that without lateral current spreading, the external differential efficiency is more temperature sensitive for this particular laser design.

5.2.2 Intrinsic Efficiency Calculated from the Differential Efficiency

An alternative method of obtaining η_d' is by examining how η_d varies with ridge width (W). This is possible by making the approximation:

$$\eta_d = \frac{q}{h\nu}\frac{dP}{dI} \approx \frac{q}{h\nu}\frac{\Delta P}{\Delta I} = \frac{q}{h\nu}\frac{\Delta P}{(\Delta I' + \Delta I_L)} \tag{5.2}$$

where ΔP is the change in output power with pumping, $\Delta I'$ is the change in the current required to produce the output, and ΔI_L is the change in lateral current with pumping.

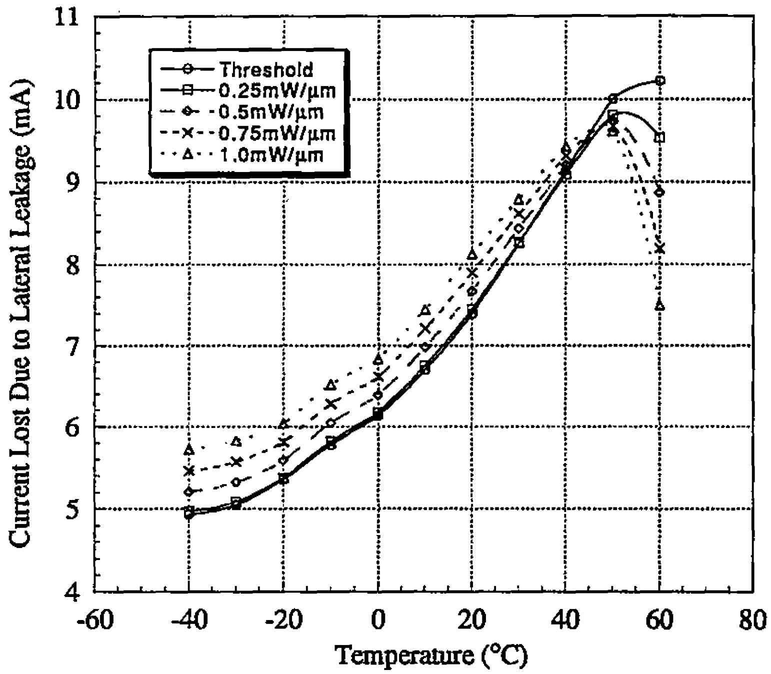

Fig. 5.4 The calculated lateral leakage for a 2µm ridge at different temperatures.

Using the fact that $\Delta I' = \Delta J' \cdot L \cdot W$ and by defining

$$\eta_d' = \frac{q}{h\nu}\frac{\Delta P}{\Delta I'} \tag{5.3}$$

it is possible to rewrite (5.2) as

$$\eta_d = \frac{W \cdot \eta_d'}{W + \dfrac{\Delta I_L}{\Delta J' \cdot L}} \tag{5.4}$$

which can be used in a two-parameter fit when η_d is plotted as a function of ridge width. To obtain the fit, it is assumed that $\Delta I_L / \Delta J' \cdot L$ is a constant, which is at least approximately valid since a linear L-I curve was obtained. Using (5.4), it is possible to obtain η_d' which is identical within error to the values calculated by using the lateral current flow model as described in Section 5.2.1. The variation of η_d' obtained from this method, along with the previous results are illustrated in Fig. 5.5. Also included is an illustration of how I_L changes with J' which is the contents of Fig. 5.6.

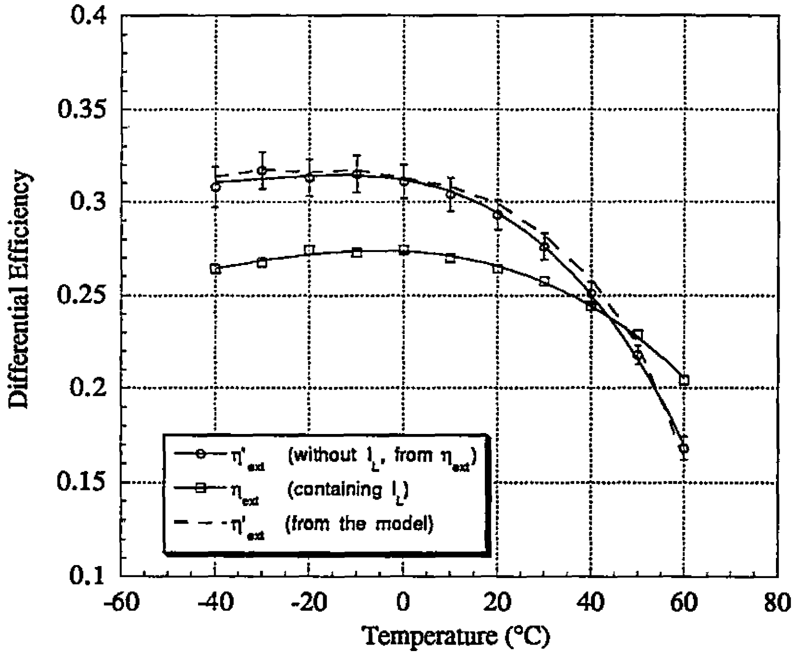

Fig. 5.5 The single facet external differential efficiency shown both with and without lateral current spreading for a 2μm ridge as derived from the measured differential efficiency.

5.3 OTHER LOSS MECHANISMS

If the lateral current spreading is ignored (or the effects removed) one can express the current density entering the laser as

$$J' = \frac{q \cdot N \cdot d}{\tau} + J_{loss} \tag{5.5}$$

where N is the average carrier density in the active region, d is the thickness of the active region, and τ is the lifetime as previously defined [Agrawal, 1993, p.126]. The lifetime

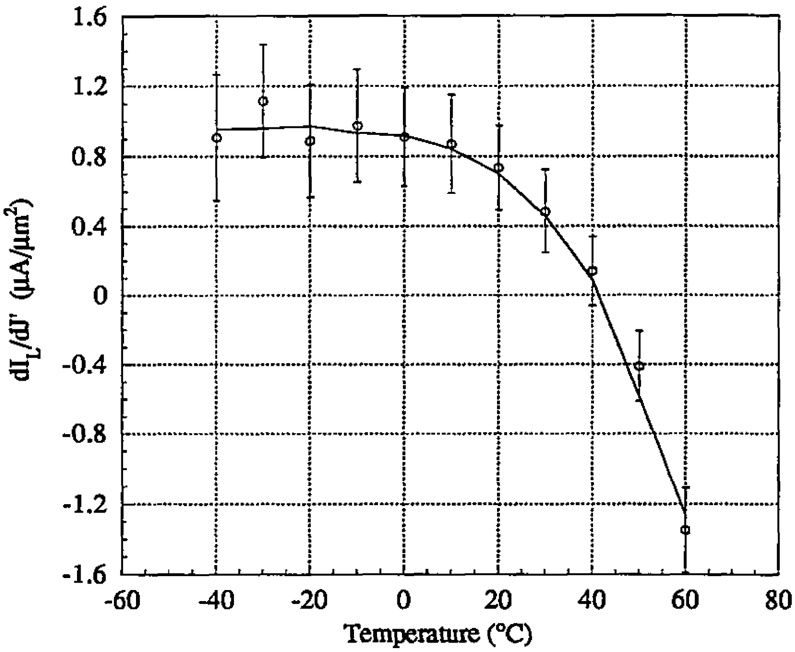

Fig. 5.6 The variation of the change of the lateral leakage (ΔI_L) over the change of the average current density ($\Delta J'$) as a function of temperature.

may be thought of as the average time that the carrier spends within the active region before it is removed by some process- either radiative or non-radiative. The J_{loss} term accounts for any loss mechanism that is independent of the current spreading rate within the active region, or more specifically, does not affect the carrier lifetime. Presumably, this is a current component which either passes through the active region, or does not enter the active region due to recombination within the ridge or waveguide.

It is a simple matter to verify (5.5) for the lasers under study by using the previously calculated diffusion length and average current density. The first step is to rewrite (5.5) in terms of L_D:

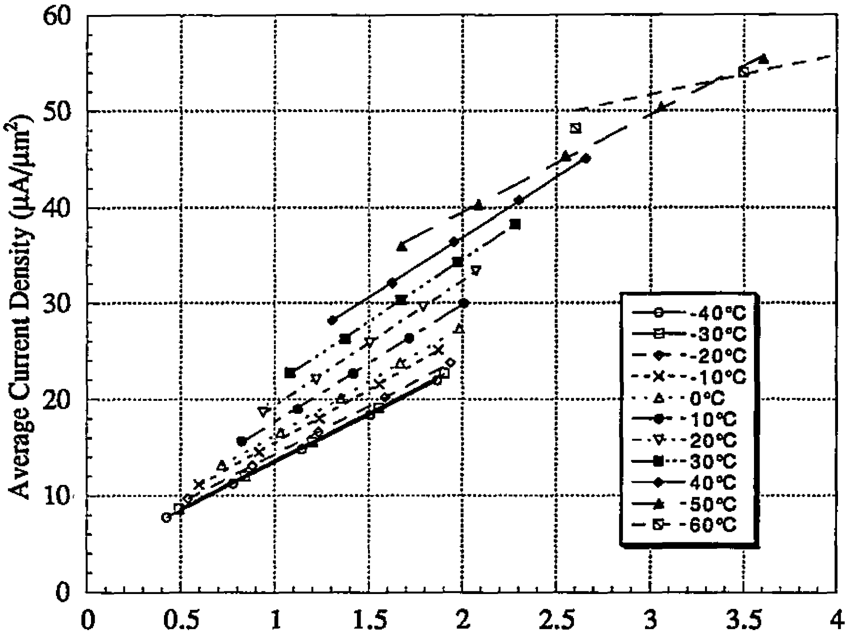

Fig. 5.7 The variation of the average current density (J') with the inverse of the square of the diffusion length (L_d) as determined from different operating points.

$$J' = \frac{q \cdot N \cdot d \cdot D_a}{L_D^2} + J_{loss} \tag{5.6}$$

Now, to verify this equation, all one has to do is find a way to vary J' and L_D without affecting D_a or N. One way that the lifetime and current density can be varied is by changing the pumping level of the laser. In such a situation, the carrier density and diffusion coefficient remain constant; and hence, a plot of (5.6) should produce a straight line. Since it was not possible to separate the ambipolar diffusion coefficient from the lifetime in the previous calculations, the diffusion length will be used instead of the carrier lifetime. Thus the slope of the graph would become $D_a{\cdot}N{\cdot}d{\cdot}q$. The results of the plot are shown in Fig. 5.7. To improve the clarity of the graph, error bars are not plotted.

(Only the error in the square of the diffusion length is significant, and it is on the order of 0.2μm^2.) Even so, the linear fits were weighted to the uncertainties within the points.

It is also useful to plot how J_{loss} varies with temperature. The result is illustrated in Fig. 5.8. Notice how this loss mechanism is approximately half of the current required to reach threshold. Note: the threshold current density illustrated here is the average current density (J') at threshold and does not contain any lateral current. The high temperature dependence of this loss mechanism emphasizes how non-radiative losses must be minimized before one can build lasers with a lower temperature sensitivity. One has to remember that the temperature quoted is that of the base of the mount for the laser. Since the actual temperature of the laser is not currently known, one has to be careful about the conclusions made about the temperature related characteristics.

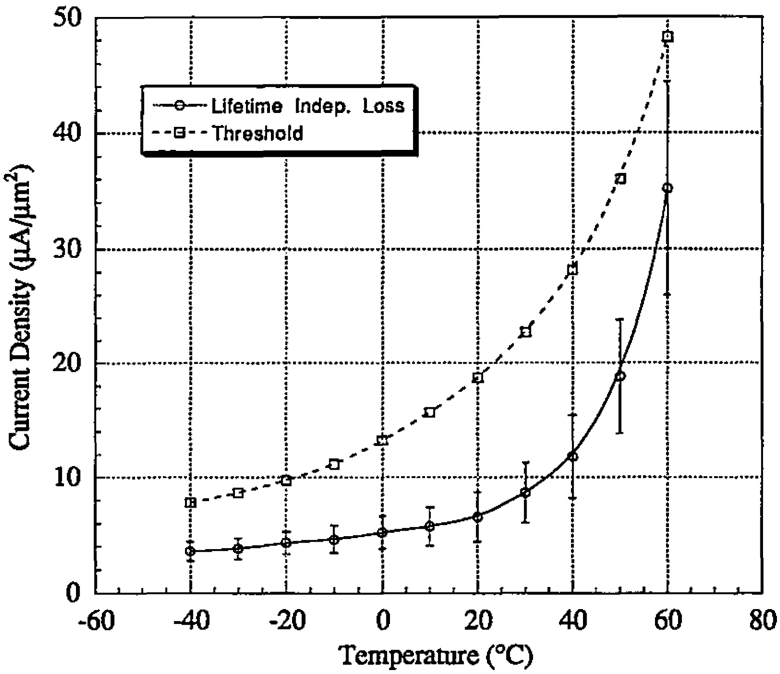

Fig. 5.8 Variation of a carrier distribution independent loss with temperature.

Figure 5.9 illustrates how the product of the carrier density and the ambipolar diffusion coefficient varies with temperature. Not much can be concluded from this graph since both of components are complicated functions of temperature. Instead, this graph is just included for completeness. One would expect that the carrier density would increase with temperature due to an increase in non-radiative loss mechanisms. At the same time, one would expect the diffusion coefficient to decrease with temperature due to a decreased mobility of the carriers due to scattering. Using the analysis of examining varying ridge width data, it does not appear to be possible to separate the diffusion coefficient from the carrier lifetime.

The results from this section must be examined with care. Once again, the diffusion length used is not the actual diffusion length within the device since the single lifetime equation (equation 3.21) is not expected to be completely valid. It is interesting to note that the linear relation between J' and $1/L_D^2$ still holds.

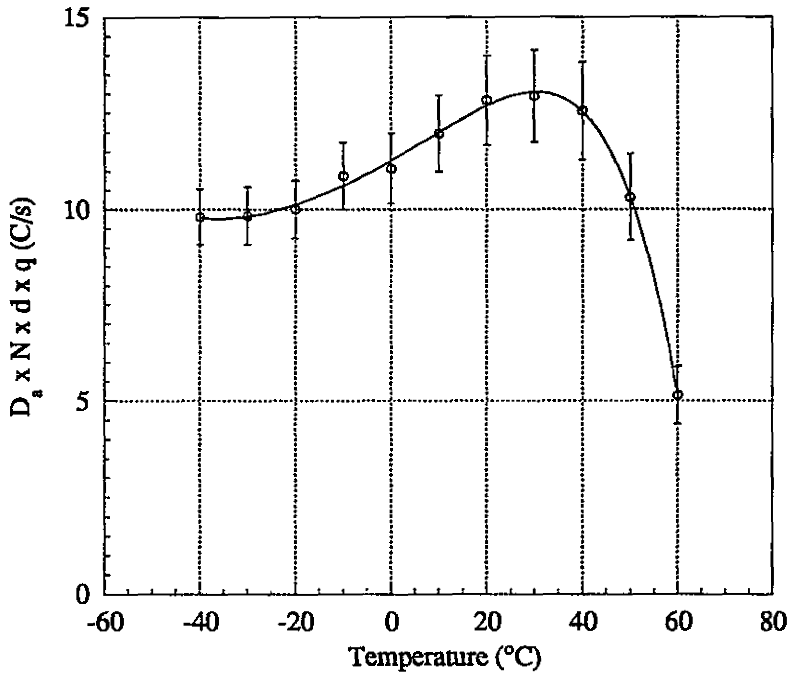

Fig. 5.9 Variation of the Diffusion Coefficient multiplied with the Carrier Density, active layer thickness and electronic charge as a function of temperature.

CHAPTER 6: SUMMARY AND CONCLUSIONS

It has been shown that lateral current spreading can be a major loss mechanism of ridge waveguide semiconductor lasers. For the *InGaAsP-InP* structure of 9 strained quantum wells examined in this thesis, as much as 60% of the total current injected into the laser at threshold is lost to the gain of the optical mode due to lateral current flow out of the active region for a ridge width of 1.5µm. As the pumping is increased, the lateral current either increases if the temperature is less than or equal to +45°C, or decreases if the temperature is greater than +45°C. This changing current affects the external differential efficiency- it is decreased at low temperatures and increased at higher temperatures, which shows that the lateral current actually decreases the temperature sensitivity of the external differential efficiency.

The optical mode is well confined under the ridge for 1.5µm or wider ridges for the structure investigated. This greatly simplifies calculations since it allows for a correlation between the ridge width and the active region to be made, and enables an analytical expression to be derived that can be used to fit the data. If smaller ridge widths were investigated, one would not be able to apply this model since the assumption of a constant lateral confinement factor for all the ridge widths would not be valid. Even so, the model suggests that smaller ridge widths could be used to produce lower threshold current lasers. However, there would be a greater temperature sensitivity since more of the optical mode is outside the injection region and hence the output will be more greatly affected by the carrier profile.

By examining the relationship between the current density under the ridge and the diffusion length, it is possible to extract a current component which is made up of non-radiative processes that do not affect the carrier profile within the laser. These processes within the *InGaAsP-InP* quantum well lasers that were examined consume approximately half of the current required to reach threshold. As well, they have a large temperature dependence which is a highly undesirable effect in communication applications.

To improve the total efficiency of the laser, one must decrease the fraction of current escaping laterally. One way this can be accomplished is by using larger ridge widths. However, this also means that larger threshold currents are required. An alternate technique is by reducing the diffusion length. Reducing the carrier lifetime is not really an option. Instead, to decrease the diffusion length, one would have to choose a material system with a reduced diffusion coefficient for holes (which would decrease the ambipolar diffusion coefficient). This would, however, have a detrimental effect on the high speed performance of the devices. The other option is, of course, to not use a ridge waveguide structure.

Lateral current spreading, and the lifetime independent loss are both major loss mechanisms in the laser structure investigated. Both of these currents have a strong temperature dependence which is detrimental to laser performance since they are such a large fraction of the injected current. These losses must be minimized if one wishes to develop low threshold, temperature insensitive, *InGaAsP-InP* quantum well semiconductor lasers.

RECOMMENDATIONS FOR FUTURE WORK

There are several improvements that should be made to the experiments so that more accurate results can be obtained. It would be useful to examine the lasers under pulsed conditions to see how much of an effect internal heating has on the results. In this way, the true temperature dependence of the loss currents can be examined and compared with theory. If this study is continued with different lasers, it would be useful to use different lengths. In that way, it would be possible to extract the internal efficiency and optical losses. It would also be interesting to try different laser structures that have a variation of active region thicknesses and compositions to see its effect on the amount of lateral carrier diffusion. A similar study will also have to be performed with 1.55μm lasers since there is currently a switch to this wavelength in progress by the communications industry.

APPENDIX I: DERIVATION OF THE AMBIPOLAR DIFFUSION EQUATIONS

Ambipolar diffusion is a common approximation used in calculating carrier profiles within semiconductors. The basis of this approximation is charge neutrality. Carriers in semiconductors consist of relatively fast moving electrons and relatively slow moving holes. As these carriers move, localized fields are created which cause the faster carriers to drag along the slower ones and hence, both carriers move at approximately the same speed. This carrier motion is described completely by the diffusion equation.

To derive the effective diffusion rate, one starts with the current equations:

$$J_n = q\mu_n\, n\xi + qD_n \frac{\partial n}{\partial x} \tag{I.1}$$

and for holes:

$$J_p = q\mu_p\, p\xi - qD_p \frac{\partial p}{\partial x} \tag{I.2}$$

In these equations, μ refers to the mobility, D is the diffusion coefficient and ξ refers to the electric field. For charge neutrality to be satisfied, the total current flowing into a region must be zero:

$$J_p + J_n = 0 \tag{I.3}$$

Substituting (I.1) and (I.2) into (I.3) yields:

$$q \cdot n \cdot \mu_n \xi + q \cdot D_n \frac{\partial n}{\partial x} + q \cdot p \cdot \mu_p \xi - q \cdot D_p \frac{\partial p}{\partial x} = 0 \tag{I.4}$$

Also, the carrier profiles for electrons and holes must be identical to satisfy charge neutrality. This means that $n=p$, and $\partial n/\partial x = \partial p/\partial x$. Using this, it is possible to solve (I.4) for the electric field:

$$\xi = \frac{D_p - D_n}{\mu_p + \mu_n} \frac{1}{n} \frac{\partial n}{\partial x} \tag{I.5}$$

This expression for the electric field is then substituted back into (I.1) and (I.2). After simplifying, this yields an expression for the electron current:

$$J_n = q \left(\frac{\mu_n D_p + \mu_p D_n}{\mu_n + \mu_p} \right) \frac{\partial n}{\partial x} \tag{I.6}$$

and for the hole current:

$$J_p = -q \left(\frac{\mu_n D_p + \mu_p D_n}{\mu_n + \mu_p} \right) \frac{\partial p}{\partial x} \tag{I.7}$$

which can be rewritten as:

$$J_n = q D_a \frac{\partial n}{\partial x} \tag{I.8}$$

and

$$J_p = -qD_a \frac{\partial p}{\partial x} \tag{I.9}$$

where D_a is defined as the ambipolar diffusion coefficient and is defined by:

$$D_a = \frac{\frac{D_p}{\mu_p} + \frac{D_n}{\mu_n}}{\frac{1}{\mu_p} + \frac{1}{\mu_n}} \tag{I.10}$$

The validity of this method is discussed in detail within a paper by Joyce [1982].

APPENDIX II: DERIVATION OF THE TWO LIFETIME MODEL

The derivation of the two-lifetime model is nearly identical to the one lifetime model. Similar to Chapter 3, the differential equation describing the carrier density is:

$$D_a \frac{\partial^2 N(x)}{\partial x^2} + \frac{J_{in}(x)}{d \cdot q} - \frac{N(x)}{\tau(x)} = 0 \qquad \text{(II.1)}$$

Rewriting (II.1) for the two regions one obtains an expression for carrier motion beneath the ridge:

$$L_{D1}^2 \frac{\partial^2 N(x)}{\partial x^2} + \frac{\tau_1 J_{in}(x)}{d \cdot q} - N(x) = 0 \qquad \text{(II.2)}$$

and one outside the ridge:

$$L_{D2}^2 \frac{\partial^2 N(x)}{\partial x^2} - N(x) = 0 \qquad \text{(II.3)}$$

where $L_{D1}(=(D_a\tau_1)^{½})$ and $L_{D2}(=(D_a\tau_2)^{½})$ are the diffusion lengths and τ_1 and τ_2 are the carrier lifetimes beneath and outside the ridge.

A solution these linear second-order differential equations can be easily found if the carrier generation rate is assumed to be zero, the system is assumed to be symmetric, and the requirement of the carrier density approaching zero as x approaches infinity is set. A solution for the equation beneath the ridge is:

$$N(x)=A\cdot\cosh\left(\frac{x}{L_{D1}}\right)+\frac{\tau_1 J_{in}}{d\cdot q} \tag{II.4}$$

and outside the ridge boundary is:

$$N(x)=Be^{\left(-\frac{|x|}{L_{D2}}\right)} \tag{II.5}$$

where A and B are constants which can be determined by applying the appropriate boundary conditions. In this situation, the boundary conditions are that the carrier profile and its derivative must be constant across the ridge boundary. Once solutions to A and B are found, it is possible to write an expression for the carrier profile. Beneath the ridge the profile is given by:

$$N(x)=\frac{L_{D2}\tau_1 J_{in}\sinh\left(\frac{W}{2L_{D1}}\right)e^{\left(\frac{W}{2L_{D2}}-\frac{x}{L_{D2}}\right)}}{q\cdot d\left[L_{D1}\cosh\left(\frac{W}{2L_{D1}}\right)+L_{D2}\sinh\left(\frac{W}{2L_{D1}}\right)\right]} \tag{II.6}$$

and outside the ridge it given by:

$$N(x)=\frac{\tau_1\cdot J_{in}}{q\cdot d}\left(1-\frac{L_{D1}\cosh\left(\frac{x}{L_{D1}}\right)}{L_{D1}\cosh\left(\frac{W}{2L_{D1}}\right)+L_{D2}\sinh\left(\frac{W}{2L_{D1}}\right)}\right) \tag{II.7}$$

These equations can be related to the recombination current density beneath the ridge (J') by:

$$J' = \frac{d \cdot q}{W} \cdot \int_{-\frac{W}{2}}^{\frac{W}{2}} \frac{N(x)}{\tau_1} dx \tag{II.8}$$

which is simply the total number of carriers beneath the ridge divided by their average lifetime beneath the ridge. After evaluation and simplification, and by using the fact that $I_{in} = J_{in} \cdot W \cdot L_c$, equation (II.8) yields an expression for the current injected into the laser:

$$I_{in} = \frac{J' \cdot L_c \cdot W \cdot \left(L_{D1} \cosh\left(\frac{W}{2L_{D1}}\right) + L_{D2} \sinh\left(\frac{W}{2L_{D1}}\right) \right)}{L_{D1} \cosh\left(\frac{W}{2L_{D1}}\right) + L_{D2} \sinh\left(\frac{W}{2L_{D1}}\right) - \frac{2L_{D1}^2}{W} \sinh\left(\frac{W}{2L_{D1}}\right)} \tag{II.9}$$

If one wishes to write the injection current as the sum of the recombination current beneath the ridge and the lateral current flow:

$$I_{in}(W) = J' \cdot L_c \cdot W + I_L(W) \tag{II.10}$$

the expression for the lateral current spreading is given by:

$$I_L = J' L \frac{2L_{D1}^2 \sinh\left(\frac{W}{2L_{D1}}\right)}{L_{D1} \cosh\left(\frac{W}{2L_{D1}}\right) + L_{D2} \sinh\left(\frac{W}{2L_{D1}}\right) - 2\frac{L_{D1}^2}{W} \sinh\left(\frac{W}{2L_{D1}}\right)} \tag{II.11}$$

which is the expression given in Chapter 3. As would be expected, (II.11) reduces to (3.23) when $L_{D1} = L_{D2}$.

REFERENCES

Agrawal, G.P., and N.K. Dutta. Long Wavelength Semiconductor Lasers. Van Nostrand Reinhold, New York, 1993.

Burkard, H. "Effective phase and group indices for $In_{1-x}Ga_xP_{1-y}As_y/InP$ waveguide structures. J. Appl. Physics. January 1984. Vol 55. No. 2. pp. 503-506.

Chiang, K.S., "Analysis of rectangular dielectric waveguides: Effective-index method with built-in perturbation correction." Electronics Letters. 1992, Vol 28. pp. 388-390.

Jones, William B., Jr. Optical Fiber Communication Systems. Harcourt Brace Jovanovich College Publishers, Fort Worth, 1988.

Hu, S.Y., S. W. Corzine, K. K. Law, D.B. Young, A. C. Gossard, L. A. Coren and J. L. Merz, "Lateral carrier diffusion and surface recombination in *InGaAs/AlGaAs* quantum-well ridge-waveguide lasers." J. Appl. Phys. 76 (8), 15 October 1994, pp 4479-4487.

Hu, S.Y., D.B. Young, A.C.Gossard, and L.A.Coren, "The Effects of Lateral Leakage Current on the Experimental Gain/Current-Density Curve in Quantum-Well Ridge Waveguide Lasers." IEEE Journal of Quantum Electronics, v30, n10, October 1994, pp 2245-2250.

Joyce, W.B., "Carrier transport in double-heterostructure active layers." J. Appl. Phys. 53(11), November 1982, pp 7235-7239.

Kapon, Eli. "Threshold current of extremely narrow semiconductor quantum well lasers." Optical Society of America, July 15, 1990, Vol.15, No.14 pp 801-803.

Suematsu, Y., Iga, K. and Kishino, K., *GaInAsP* Alloy Semiconductors. Edited By T.P. Pearsall, John Wiley & Sons Ltd. New York, 1982.

Tamir, T. ed. Integrated Optics. Springer-Verlag Berlin Heidelberg: Germany, 1975.

Walpita, L.M., "Solutions for planar optical waveguide equations by selecting zero elements in a characteristic matrix." J. Opt. Society of America. A., 2(4), pp. ~~2~~95-
595
602, 1985.

Wolf, C. N. Holonyak, G. Stillman, Physical Properties of Semiconductors. Prentice Hall: New Jersey, 1989.

Zory, P.S. Jr. ed., Quantum Well Lasers. Boston: Academic Press, Inc., 1993.